

https://dspace.org/

Dust penetrated quantitative classifcation of nearby barred spiral galaxies

Tailor, Asha

2012-09-12
http://hdl.handle.net/10539/11934

Downloaded from a DSpace repository. https://dspace.org/

Dust Penetrated Quantitative Classification of Nearby Barred Spiral Galaxies

Asha Tailor

A Dissertation submitted to the
School of Computational and Applied Mathematics,
Faculty of Science,
University of the Witwatersrand,
in fulfilment of the requirements for the degree of
Master of Science.

Johannesburg, December 2011.

DECLARATION : I declare that this dissertation is my own, unaided work. It is being submitted for the degree of Master of Science at the University of the Witwatersrand, Johannesburg. It has not been submitted before for any degree or examination to any other University.

_____

(Signature)

_____

(Date)

Dedicated to my Loving parents, Sisters, best friend Dario and my Mentor, Dr. Robert Groess

Contents

Acknowledgements **v**

Abstract **vi**

List of Figures **vii**

List of Tables **xiii**

1 Classical Morphology **1**

1.1 Early pioneers in Galaxy Classification 1

1.2 The Hubble Classification Scheme 2

1.2.1 Reynolds' Continuum 2

1.2.2 Jeans' Tuning Fork Diagram 4

1.2.3 Extensions of "Hubble's" classification system 7

1.3 Quantitative Classification 9

1.3.1 The near infrared Window 9

1.3.2 Quantifying Bars 10

2 Ubiquity of the Bar Phenomenon **12**

2.1 Importance of Bars 12

2.2 The Bar life-cycle 14

2.3 Morphological importance of Dust in Barred galaxies 18

2.4 Bars in the near infrared 22

2.5 Quantitative Measures of Bar Strength 24

2.6 Relative Gravitational Torques 26

3 Gravitational Torque Method **30**

3.1 Introduction 30

3.2 Getting the Potential 31

3.3 Calculating Force Ratios 32

3.4 The Sample 34

3.5 Preprocessing 37

3.6 Results & Discussion 39

4 Isophotal Ellipses **49**
4.1 Galactic Isophotes 49
4.2 Properties of S^{4}G galaxies 51
4.3 Ellipse Fitting Method 53
4.4 Step by Step Procedure 54
4.5 Results & Discussion 56

5 Conclusion **61**
5.1 Looking back 61
5.2 Relative Maximum Gravitational Torques 63
5.3 Isophotal Ellipses 63
5.4 Future Focus 64
5.5 Final words 64

A Appendix **66**
A.1 Image alignment & Cleaning 66
A.2 Image Scale and Size 67
A.3 Deprojecting Images 67

References **76**

ACKNOWLEDGEMENTS

I want to thank the Square Kilometer Array bursary program for generous funding which has made the research in this dissertation possible, as well as the opportunity of meeting other astronomers in South Africa through the annual SKA bursary conference.

I also want to thank my mentor Dr. Robert Groess for always inspiring me, as well as guiding me. The journey from the beginning 'till the end has been an awesome one, thank you. Your guidance and inspiration is truly appreciated.

I thank the S^4G team for their kind collaboration and providing data essential for the ellipse fitting analyses.

I would also like to thank my friend Dario who has been there to listen to all my complaints, and to inspire me and for making me believe in myself.

And my parents for supporting my decision in studying further as well as putting up with my music while I worked late nights. I apologize to my sisters for being away while trying to complete my dissertation. Thank you for your understanding. My little nieces Arpita and Tia, and nephew Chirag, thank you for giving me the best break ever from working.

Finally, everyone in the lab, Obakeng, Viren, Franklin, Elimboto, Sima, Terry, Tanya, Tumelo and Morgan for making the working environment a fun place to be.

ABSTRACT

The objective of this dissertation is twofold. Firstly an extensive yet concise literature review on the state-of-the-art of near infrared barred spiral galaxy classification is presented. Secondly, two quantitative approaches to galaxy classification at near infrared wavelengths, the relative gravitational torque method and the isophotal ellipse fitting method, are applied for the first time to a sample of selected Spitzer IRAC nearby barred galaxies. Maximum relative gravitational torques are derived for a sample of 40 nearby bright barred disk galaxies at 3.6μm and 4.5μm. These torques are compared between galaxy pairs at these passbands and we find an excellent agreement between the 3.6μm and 4.5μm morphology. The sample used incorporates a wide range of inclination and bar strength values. The tight coupling of 3.6μm and 4.5μm morphology provides an opportunity to classify intermediate redshift galaxies that have their near-infrared rest frame emissions shifted red-ward to 4.5μm; i.e.: out to $z = 0.25$. We find a greater frequency of higher maximum relative torques in our sample compared with either Block et al. (2002) or Buta et al. (2004) due to sample bias, as this dissertation is aimed at understanding quantitative methods in classifying barred galaxies. Furthermore, we compare results from applying an isophotal ellipse fitting technique and a gravitational torque analysis to a common sample of 28 nearby barred S^4G/Spitzer galaxies imaged at 3.6μm. These two quantitative bar strength methods are applied to images that have identical orientation and deprojection parameters for an objective comparison. We find a strong correlation between the gravitational torque and isophotal ellipse fitting methods which in principle supports a method for estimating bar potentials out to intermediate redshifts by using an isophotal ellipse fitting approach. This has important implications for bar-fraction estimates and galaxy accretion/evolution scenarios.

List of Figures

1.1 Wolf's descriptive classification scheme (1908) of 17 morphological bins, (g) through (w). Like-appearing objects were grouped according to their observed morphology. 2

1.2 Hubble's *original* tuning fork diagram as published in 1936 in his *Realm of the Nebulae, pp. 45.* The tynes of the tuning fork represent continuity between the separate branches of barred and non-barred spiral forms. 5

1.3 Jeans' tuning fork diagram as published in 1929 in his *Astronomy and Cosmogony.* The placement of objects along the continuous sequence is likely to have been the inspiration for Hubble's own version of the tuning fork diagram - rotated 90° clockwise from that of Jeans'. 6

1.4 Schematic representation of the de Vaucouleurs classification volume. In this scheme the primary classification parameter is the Hubble E-Im continuum. The second parameter relates to the presence (SB) or absence (SA) of a bar. The third distinguishes between ring (r) and spiral (s) varieties. The second and third parameter effects are largest near Hubble stage Sa. 8

2.1 The bar dissolution/rejuvenation cycle: Interplay between gas accretion and secular evolution. External gas accretion drives the formation of bars, moving galaxies towards the lower-right. Secular evolution dissipates bars, and tends to evolve galaxies to upper-left. (Bournaud & Combes 2004). 17

3.1 Preparation for Deprojection of NGC1300 38

(a) Original Image 38

(b) Centred 38

(c) Star Cleaned 38

(d) Deprojected 38

3.2 Centered, star-cleaned, deprojected, $2^n \times 2^n$ dimensional image of NGC1300 as required for Potential calculation by Quillen, Frogel & González (1994). 39

3.3 The distribution of maximum relative gravitational torques of image pairs between $3.6\mu m$ and $4.5\mu m$. There is a tight coupling of morphology in all galaxy pairs in our sample across a wide range of Q_g values. . . . 40

3.4 Observed number frequency of $3.6\mu m$ (solid line) and $4.5\mu m$ (dotted line) gravitational torques in our sample. 41

3.5 Torque maxima positions for $3.6\mu m$ and $4.5\mu m$ image pairs. 45

NGC0289($3.6\mu m$) 45

NGC0289($4.5\mu m$) 45

NGC0600($3.6\mu m$) 45

NGC0600($4.5\mu m$) 45

NGC0613($3.6\mu m$) 45

NGC0613($4.5\mu m$) 45

NGC0685($3.6\mu m$) 45

NGC0685($4.5\mu m$) 45

NGC0936($3.6\mu m$) 45

NGC0936($4.5\mu m$) 45

NGC0986($3.6\mu m$) 45

NGC0986($4.5\mu m$) 45

NGC1300($3.6\mu m$) 45

NGC1300($4.5\mu m$) 45

NGC1326($3.6\mu m$) 45

NGC1326($4.5\mu m$) 45

NGC1365($3.6\mu m$) 45

NGC1365($4.5\mu m$) 45

NGC1398(3.6μm) 45

NGC1398(4.5μm) 45

3.5 Torque maxima positions for 3.6μm and 4.5μm image pairs (Continued). 46

NGC1433(3.6μm) 46

NGC1433(4.5μm) 46

NGC1493(3.6μm) 46

NGC1493(4.5μm) 46

NGC1512(3.6μm) 46

NGC1512(4.5μm) 46

NGC3198(3.6μm) 46

NGC3198(4.5μm) 46

NGC3319(3.6μm) 46

NGC3319(4.5μm) 46

NGC3368(3.6μm) 46

NGC3368(4.5μm) 46

NGC3504(3.6μm) 46

NGC3504(4.5μm) 46

NGC3513(3.6μm) 46

NGC3513(4.5μm) 46

NGC3627(3.6μm) 46

NGC3627(4.5μm) 46

NGC3892(3.6μm) 46

NGC3892(4.5μm) 46

3.5 Torque maxima positions for 3.6μm and 4.5μm image pairs (Continued). 47

NGC4245(3.6μm) 47

NGC4245(4.5μm) 47

NGC4394(3.6μm) 47

NGC4394(4.5μm) 47

NGC4421(3.6μm) 47

NGC4421(4.5μm) 47

NGC4450(3.6μm) 47

NGC4450(4.5μm) 47

NGC4535(3.6μm) 47

NGC4535(4.5μm) 47

NGC4548(3.6μm) 47

NGC4548(4.5μm) 47

NGC4593(3.6μm) 47

NGC4593(4.5μm) 47

NGC4596(3.6μm) 47

NGC4596(4.5μm) 47

NGC5101(3.6μm) 47

NGC5101(4.5μm) 47

NGC5371(3.6μm) 47

NGC5371(4.5μm) 47

3.5 Torque maxima positions for 3.6μm and 4.5μm image pairs (Continued). 48

NGC5375(3.6μm) 48

NGC5375(4.5μm) 48

NGC5383(3.6μm) 48

NGC5383(4.5μm) 48

NGC5921(3.6μm) 48

NGC5921(4.5μm) 48

NGC6217(3.6μm) 48

NGC6217(4.5μm) 48

NGC6744(3.6μm) 48

NGC6744(4.5μm) 48

NGC7329(3.6μm) 48

NGC7329(4.5μm) 48

NGC7479(3.6μm) 48

NGC7479(4.5μm) 48

NGC7552(3.6μm) 48

NGC7552(4.5μm) 48

NGC7741(3.6μm) 48

NGC7741(4.5μm) 48

IC1438(3.6μm) 48

IC1438(4.5μm) 48

4.1 Isophotal ellipse contours for increments in radius superimposed over a 3.6μm deprojected image of NGC1300. Ellipse contours have the highest ellipticity over the bar region, the maximum of which is used to define ϵ_{max}. 55

4.2 Ellipticity and Position angle profiles of NGC5101 reveal the signature of a bar as defined by the following criteria: Ellipticity increases monotonically as a function of the semi-major axis radius until reaching a maximum (ϵ_{max}) - the bar strength. The position angle remains fairly constant within this bar region. NGC 5101 has a bar strength of 0.6. . 55

4.3 Number frequency of barred galaxies with bar strength defined in terms of maximum relative gravitational torque (solid line) and isophotal bar axis ratio, $b/a = 1 - \epsilon_{max}$ (dashed line). The results are consistent with our sample being biased towards nearby bright barred galaxies. 59

4.4 Comparison of maximum relative gravitational torques (Q_g) with maximum isophotal ellipticity values (ϵ_{max}). There is a good correlation between these bar strength measures for our sample where identical positions, deprojection and orientation parameters were used for each technique. The sharp minimum cutoff evident at $(b/a) \sim 0.3$ is attributed to the specific geometry of the bar phenomenon. Very long thin bars are not observed at any wavelength. 60

List of Tables

3.1 Bar strength classes defined by Buta & Block (2001) 34

3.2 Properties of the GTM Sample 35

3.3 Maximum Relative Gravitational Torque 42

4.1 Properties of the S^4G sample (T&F = Tully & Fisher 1987 ; T= Tully 1988) 52

4.2 Bar Strengths described by Q_g and ϵ_{max} 58

Chapter 1

Classical Morphology

"Great things are not done by impulse, but by a series of small things, brought together."

-Vincent van Gogh

1.1 Early pioneers in Galaxy Classification

Early 19th century pioneer, Sir William Herschel was among the first to attempt a comprehensive description and classification of a wide range of "nebulae" based on brightness, form and size. This description was further extended by his son, Sir John Herschel making a clear distinction between galactic and non-galactic nebulae. These are now known as nebulae and galaxies, respectively. The Herschels' catalogue comprises nebulae and clusters of stars with 5079 entries of which 4630 were discovered by the Herschels themselves and was published in 1864 by John Herschel. This subsequently formed a large basis of the New General Catalogue (NGC) of Johan L.E. Dreyer (1888) which contains the descriptive symbols used by the Herschels in their introduction.

A better descriptive scheme was engineered by Wolf (1908) who proposed 17 morphological bins labelled (g) through (w) (see Figure 1.1), based on photographs taken at Heidelberg, Germany. Wolf's scheme however, in addition to the Herschels' description, described dust lanes, projected ellipticities, and spiral patterns. This descriptive scheme provided a simple way of arranging nebulae into like-appearing objects making the system very comprehensive. Indeed, most optical nearby spiral galaxies today, can easily be arranged in the Wolf system - with the exception of dwarf galaxies.

The descriptive schemes of the Herschels and Wolf impose a discrete set of possibilities for classification and require that each galaxy under scrutiny fall into one of the

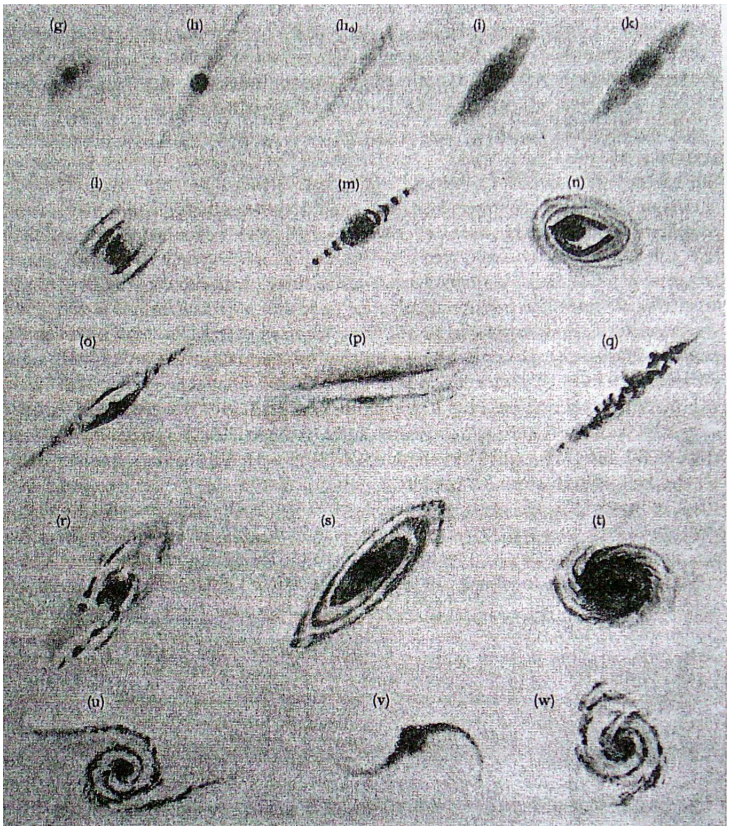

Figure 1.1: Wolf's descriptive classification scheme (1908) of 17 morphological bins, (g) through (w). Like-appearing objects were grouped according to their observed morphology.

pre-set categories. There is no space for an object that is part-way between different classes because there is no implied ordering between the morphological bins in these models.

1.2 The Hubble Classification Scheme

1.2.1 Reynolds' Continuum

In the early 20th century, John H. Reynolds (1920) suggested a morphological continuum of spiral forms. He studied surface-brightnesses of galaxies by measuring the bulge profiles with different luminous spatial bulge to disk ratios, and derived an equation that shows surface brightness decreases from the centre of a galaxy, outwards, as follows:

$$(1+x)^2 I(r) = constant \tag{1.1}$$

where $I(r)$ is surface brightness, r is radius, and x is distance along the major axis

Reynolds then placed these in sequence of forms, such that the characteristics changed continuously from one class to another. These he labelled classes I to VII, which are described below in his own words:

I. "Spirals consisting entirely of amorphous nebulosity"

II. "Spirals showing incipient condensations in the outer whorls only"

III. "In this class the condensation in the outer region has advanced considerably towards the nucleus. This is the stage reached by NGC3031 ... where the outer half is of the condensed type, including what appear to be actual star disks, while the nuclear region is of the amorphous type and has a light distribution similar to the Andromeda Nebula."

IV. "Includes the great majority of spirals. The nebular condensations appear in all regions except the nucleus itself, but a hazy background is still more or less conspicuous."

V. "An advanced stage of Class IV: the whole nebula is of the condensed type, the nucleus often having a definite boundary like a planetary nebula. The hazy background has practically disappeared in all the regions."

VI. Reynolds describes nebulae of the intermediate type, with outer rings and "condensations" in the inner arms.

VII. "Spirals of the course granular type which have no definite nucleus at all, such as NGC253..."

Soon afterwards, Hubble published a classification scheme in his 1926 landmark paper, which is his only technical paper on the classification of spiral galaxies. Here Hubble uses photographic (optical) images to distinguish elliptical, spiral, and irregular types; with spiral galaxies further divided into barred and unbarred variants: (SBa, SBb, SBc) and (Sa, Sb, Sc) respectively.

Hubble's classification scheme is simple yet considers a wide range of morphology observed in spiral nebulae. This classification is according to three criteria: the size of the central bulge, the degree of resolution in the arms, and the openness of the spiral arms.

Comparing Hubble's scheme with that of Reynolds', it is clear that Hubble's Sa, Sb, early Sc and later Sd are identical to Reynolds' continuum I-VII. The similarity of these two schemes were noted by Sandage (2005) who asserts the "correspondence is one-to-one". In fact, Hubble's second criteria is in the language of Reynolds' scheme (1920), yet Reynolds' name appears nowhere in Hubble's 1926 paper, nor in his comments (Hubble, 1927) to Reynolds' criticism, where Reynolds had called Hubble's attention to his 1920 paper.

Reynolds criticised Hubble's scheme as being too 'simple' (Reynolds, 1927), ''This classification of spirals seems to me to be altogether too simple for the great range of types", when he himself proposed a classification very similar to that of "Hubble's" scheme in his 1920 paper. He argued that Hubble's scheme lacked much of the detail exhibited by galaxies, which he believed a classification should account for. He insisted that a classification should accommodate characteristics such as the extent to which spiral arms wind around the bulge, as well as the strength or "massiveness" of the spiral arm patterns. It is not clear what motivated Reynolds to condemn Hubble's scheme as being too simple, when it was in fact a reformulation of his own work. The key point that Reynolds had failed to notice about his scheme - the continuum classification of galaxies - is precisely what lends such extraordinary strength to Hubble's legacy. The simplicity of Hubble's classification system is what makes it elegant and still proves to be useful today. It does not branch off to classify parameters which do not form part of a continuum separately, variations such as luminosity and arm/interarm density. Hubble (1926) believed that these were too small compared with "the path of the sequence". Had Reynolds not repudiated his involvement in the ground work to Hubble's classification system, "Reynolds would now have been considered as an early originator of part of the modern classification" (Sandage, 1975).

1.2.2 Jeans' Tuning Fork Diagram

Another element may well have led to the true dominance of Hubble's system. In 1936, Hubble's classification was graphically presented in his popular book, "Realm of the

Nebulae", in the form of the now famous "Hubble Tuning Fork" (Figure 1.2). This diagram depicts elliptical galaxies at the left end of the Tuning Fork and evolves to the right as Spiral galaxies; labelled by Hubble as "early type galaxies" and "late type galaxies", respectively.

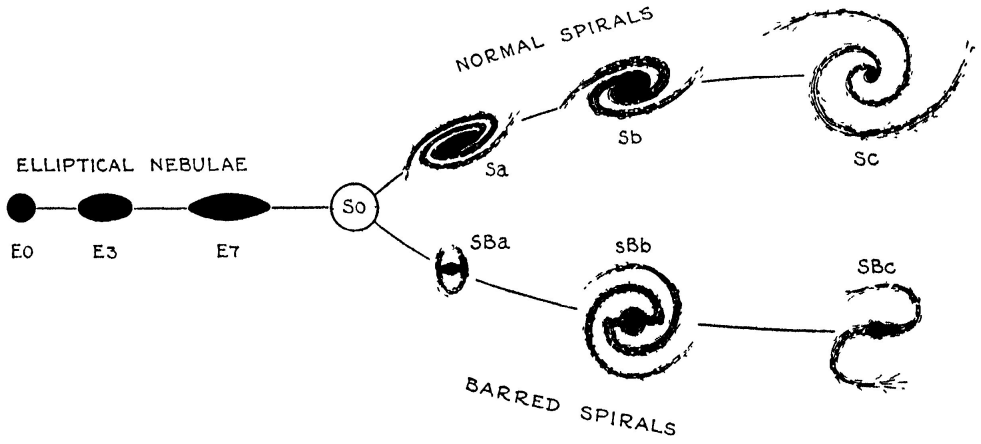

Figure 1.2: Hubble's *original* tuning fork diagram as published in 1936 in his *Realm of the Nebulae, pp. 45.* The tynes of the tuning fork represent continuity between the separate branches of barred and non-barred spiral forms.

From the comparison of Reynolds' scheme (1920) to that of Hubble's (1926), it is quite clear that the origin of the latter is based on work done by the former. However, the origin of the Tuning Fork diagram itself is a mystery, for it was not presented with the scheme in 1926 but after 10 years in 1936. A hint for its origin may be found in Jeans' (1919) Smith Prize Essay, *"Problems of Cosmogony and Stellar Dynamics"*, in which Jeans illustrates the separation of spiral galaxies into two separate sequences. Jeans was inspired by the discovery of the rotation of galaxies and speculated that the flattened structures of the nebulae was due to evolution of gaseous or possibly even liquid bodies, all dependent upon their rotation rate.

Jeans (1929) read Hubble's 1926 paper, and had well understood Hubble's description of classification. He then summarized Hubble's scheme, in his book *Astronomy and Cosmogony* 1929, by representing a diagram, which shows a linear sequence of elliptical galaxies and two tynes of a tuning fork separating ordinary and barred spirals (Figure 1.3). If this is compared to Hubble's Tuning Fork (Figure 1.2), it is quite clear that Hubble had rotated Jean's diagram by 90°, added graphics of the opening of arms in the spiral sequence, the progressive flattening sequence of the elliptical galaxies, and

then the hypothetical S0 galaxies, which resulted in what is now known as the Hubble Tuning Fork.

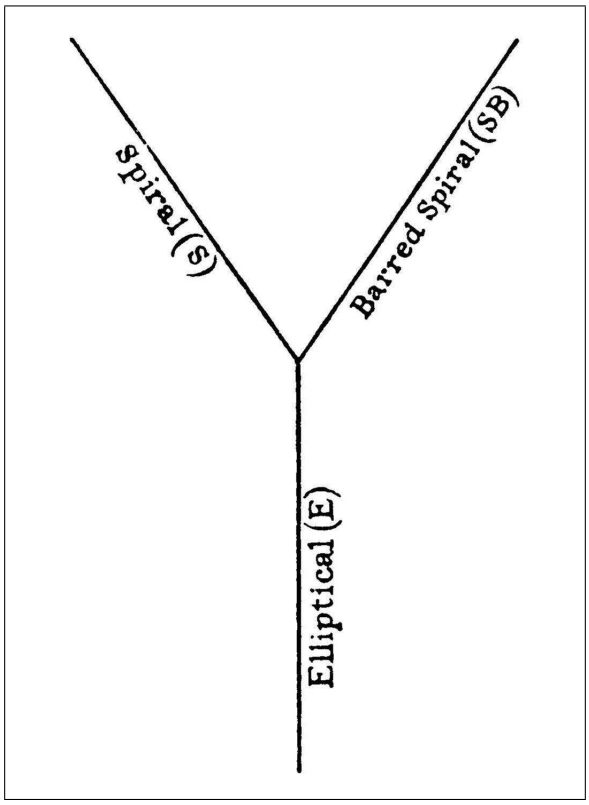

Figure 1.3: Jeans' tuning fork diagram as published in 1929 in his *Astronomy and Cosmogony*. The placement of objects along the continuous sequence is likely to have been the inspiration for Hubble's own version of the tuning fork diagram - rotated 90° clockwise from that of Jeans'.

Block in his *Shrouds of the Night*, (2008) suggests the diagram should be called "*The Hubble-Jeans Tuning Fork"*, because it was Jeans who initially thought of representing the Hubble scheme in the form of a diagram, which greatly aids the *notion of continuity*.

The classification of nebulae into two different classes was recognized by Knox-Show (1915), Curtis (1918a), Reynolds (1920) and particularly Lundmark (1926), before Hubble (1926). The only difference between Hubble's classification of nebulae and Lundmark's is that Hubble classified his nebulae as Elliptical and Spiral, whereas Lundmark classified them as galactic and anagalactic nebulae, denoting them G and A respectively. The type A galaxies were further subdivided into what Lundmark called globular, elliptical, elongated, ovate, and lenticular morphologies. He also proposed the class "Magellanic nebulae", denoting them as Am. He then subdivided this group into six degrees of "compression" towards the centre. Similarly, he ordered his final class,

"spiral nebulae", in terms of "compression towards the centre".

For this Hubble boldly accuses Lundmark of plagiarism (in foot note 2, on page no. 323 of Hubble's 1926 paper) "*Dr. Lundmark makes no acknowledgements or references to the discussion ... other than those for the use of the term 'galactic'.*" However, this is not true as Lundmark (1927) was particularly careful, and pointed out, "*Hubble classifies his subgroups according to excentricity or form of the spirals or degree of development while I use the degree of concentration towards the centre ...*".

1.2.3 Extensions of "Hubble's" classification system

Hubble introduced further continuity between the S0 and SBa galaxies in an unpublished reapportionment, which was found by Sandage and Humason after Hubble's death. Here Hubble sub-divided his Sa galaxies, from his 1936 system, into S0 and revised Sa classes. He also regrouped the original SBa galaxies into the SB0 class, and the SBb galaxies into the new revised SBa or SBb class. These new Hubble bins were published by Sandage (1961) in the *Hubble Atlas of Galaxies*.

One additional significant modification was pioneered by de Vaucouleurs (1956), by introducing the concept of a classification *volume*. The classification volume stipulates "family" and "variety" relating to the presence (and absence) of a bar and of an inner ring, respectively. Pure ring systems were denoted (r), and "spiral arm subtypes" were represented with (s). His three dimensional classification is represented in Figure 1.4, where the horizontal dimension represents the continuity of forms along the sequence E-E$^+$-S0$^-$-S0^0-S0$^+$-Sa-Sb-Sc-Scd-Sd-Sdm-Sm-Im, and the vertical dimension, as in the Hubble Tuning Fork diagram, differentiates between galaxies with no bars (SA), galaxies with weak bars (SAB) and galaxies with strong bars (SB). The third dimension distinguishes between objects that exihibit r and s varieties.

However a simpler classification scheme, compared to that of Hubble, was formulated by Morgan in 1958. His classification scheme is a one-dimensional system based on central concentration of light. He arranged galaxies in a sequence *a-f-g-k*, with a representing the weakest central concentration of light and k having the strongest.

Further noteworthy classifications were made by the following authors. Van den Bergh (1960) introduced a "luminosity class" and illustrated the "beauty" or "regularity" of spiral disks, which essentially relates to the degree of symmetry exhibited by

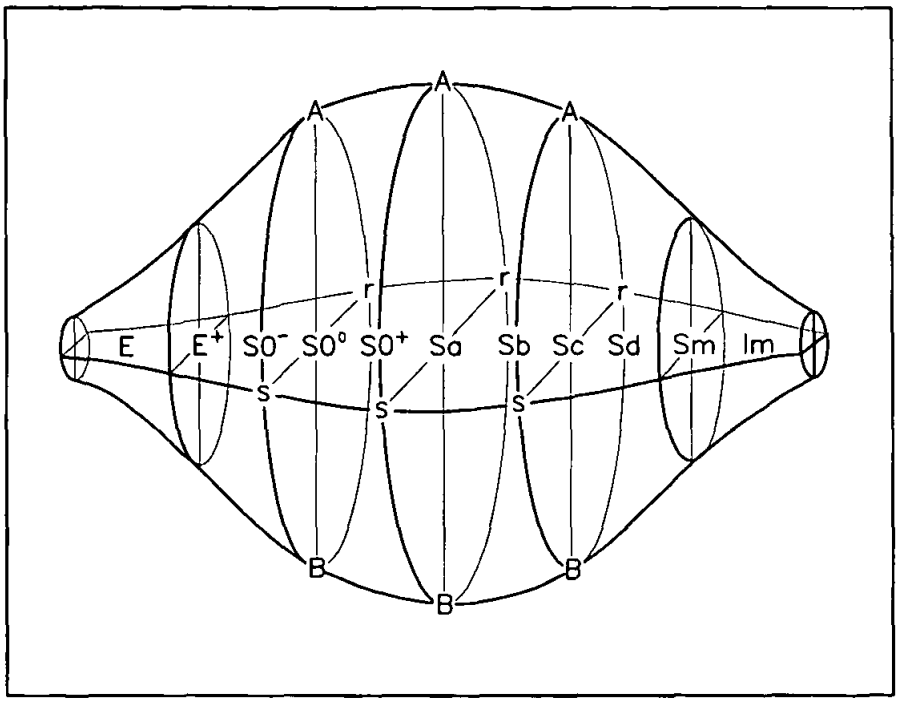

Figure 1.4: Schematic representation of the de Vaucouleurs classification volume. In this scheme the primary classification parameter is the Hubble E-Im continuum. The second parameter relates to the presence (SB) or absence (SA) of a bar. The third distinguishes between ring (r) and spiral (s) varieties. The second and third parameter effects are largest near Hubble stage Sa.

a particular galaxy. Vorontsov-Velyaminov et al. (1962-1974) classified thousands of galaxies using a descriptive scheme that greatly expanded the Wolf system by providing much detail in the notations.

The above-mentioned schemes are all based on blue light images and are purely descriptive, but fail to relate to the underlying physics which governs the morphology of galaxies. They do not explicitly consider the effects of relative bulge size and the presence of bars on the dynamics of galaxies.

A somewhat different approach was taken by Elmegreen & Elmegreen (1982,1987) who devised a twelve-stage classification system for spiral arms. These classifications range from Type 1 "flocculent" arms that are ragged, patchy, or chaotic to Type 12 "grand design" arms, which are long, symmetrical, sharply defined and dominate the appearance of the spiral galaxy in which they occur.

1.3 Quantitative Classification

1.3.1 The near infrared Window

Early astronomers studied galaxy morphology by means of visual observations. Some aspects of galaxy morphology classification were learned through sketches of galaxies and many more from the images of galaxies recorded on blue photographic plates. Pioneers during this era had recorded many galaxies and classified them, according to their *apparent* features. As a result galaxy classification "remained subjective, requiring experts to manually classify [them]" (Wijesinghe et al. 2009).

More recently 10m class observatories as well as space-borne telescopes have become available equipped with photometers, CCDs, and infrared camera arrays. Since these detectors capture data in numerical form, it became possible to perform rigorous mathematical analyses on images of galaxies and the purely descriptive subject of galaxy morphology has now become quantitative.

The advent of near infrared (NIR) imaging has made it possible to numerically classify galaxies as these images can be used to derive the gravitational potential of their mass distribution. NIR images are tracers of mass distribution, due to their emphasis on the older, dominant stellar population (Rix & Rieke 1993; Block et al. 1994; Buta et al. 2003b), thus revealing the "stellar backbone" of galaxies. This affords us the opportunity to make use of physical properties of galaxies as the basis for a classification scheme. Sanders & Tubbs (1980) and Combes & Sanders (1981) suggest that the gravitational potential of the mass distribution can be used to determine the radial and tangential force. These authors provide a quantitative classification of gravitational torques in terms of the maximum ratio of the tangential force to that of the mean axisymmetric radial force. However, *measuring* the gravitational potential of galaxies only became possible nearly a decade later, when Mercury Cadmium Teluride (HgCdTe) NIR detectors became available. Potentials from these NIR images of galaxies can be derived using the Fast Fourier Transform techniques of Quillen, Frogel, and González (1994), thus revealing a single dimensionless parameter, the relative gravitational torque, Q_g. This method is commonly known as the Gravitational Torque Method (GTM).

1.3.2 Quantifying Bars

The GTM was first applied by Buta & Block (2001) to a sample of J- and H-band images of nearby *barred* spirals from the WHT (William Herschel Telescope). These authors introduced a full continuum of "bar strengths" based on the gravitational forcing of the bar itself. The following bar strength classes were recognized: bar class 0 galaxies, which are normal spiral galaxies without any bar; bar class 1 and 2 galaxies, which show oval and weak bars; and bar class 2-7, which encompass all galaxies classified as SB by Hubble and de Vaucouleurs.

Further application of the GTM was undertaken by Laurikainen & Salo (2002) using JHK images from 2MASS. They applied two different numerical methods, a direct cartesian integration method and a polar grid integration, to determine the gravitational potential and found that bar strength measurements were independent of the method used. Laurikainen, Salo & Rautiainen (2002) also applied the GTM to JHK images from 2MASS to compare bar strengths of active and non-active galaxies. The GTM was further used to study the distribution of bar strengths (Block et al. 2002; Whyte et al. 2002; Buta et al. 2004; Buta et al. 2005). Block et al. (2004) investigated the relation between bar torques and spiral arms, by applying the GTM to K_s-band images from the WHT sample. Bar strength measured at $3.6\mu m$ and $8.0\mu m$ images from Spitzer were compared by Groess (PhD Thesis 2007) for the purpose of understanding dust morphology in emission at $8.0\mu m$.

This dissertation will focus on extending the range of previous surveys by performing analyses on both the IRAC 3.6μm and 4.5μm channels and comparing the results in a region where the Rayleigh-Jeans tail experiences a notable drop-off from stellar objects. Images at these wavelengths trace the older population I stellar backbone of disk galaxies, and also do not suffer from excessive attenuation due to dust. Using the constant mass to light ratio assumption allows us to see the dynamical mass of the galaxy and hence calculate gravitational torques. Secondly, a relationship between pure isophotal classification (such as an ellipse fitting method) and that of the GTM are investigated.

To this end a specialized set of nearby galaxy images from IRAC Principle Investigator, Dr. Giovanni Fazio at the Harved-Smithsonian Centre for Astrophysics, will be analyzed. The GTM will be applied to a select sample of 40 galaxies in both 3.6μm and 4.5μm by making use of the IRAF package as well as some specialized code written

in C and Fortran.

Furthermore a comparison of the Gravitational Torque method with an isophotal ellipse fitting method, may well provide insight into the relationship between gravitational torques and the luminous contribution of bars at near-infrared wavelengths. The sample of galaxies described above with others from the Spitzer Survey of Stellar Structure in Galaxies (S^4G) will also be used to perform an isophotal ellipse fitting analysis. A relationship between the two quantities Q_g and ϵ_{max} (both parameters lying between 0 and 1) will be investigated at $3.6\mu m$. This would provide a method to estimate gravitational torques of more distant galaxies at rest frame $3.6\mu m$, where the data is more noisy. The maximum value of ellipticity was obtained by analyzing the ellipticity and position angle profiles to classify galaxies as barred or unbarred. The two parameters Q_g and ϵ_{max} are then compared to find a relationship between them.

The following chapter *Ubiquity of the Bar Phenomenon* discusses the importance of bars in galaxy classification, the life cycle of bars, the influence of dust in barred galaxies, and the phenomenon of bars at near infrared wavelengths, by means of a brief literature review. In here, we also discuss the importance of classifying galaxies according to their bar strengths using quantitative methods. These quantitative methods are further described in Chapter 3 and Chapter 4 with their applications. Chapter 3 describes the gravitational torque method and its application to 40 Spitzer IRAC galaxies followed by a comparison of maximum torques measured at $3.6\mu m$ and $4.5\mu m$. Chapter 4 describes the Isophotal Ellipse fitting method and its application to a subsample of 28 S^4G/Spitzer galaxies. This chapter ends with a discussion of a correlation between the two quantitative methods and a comparison with similar results in the literature. Finally the dissertation will be concluded, future work will be discussed and an exhaustive bibliography will be provided.

Chapter 2

Ubiquity of the Bar Phenomenon

"With increasing distance, our knowledge fades, and fades rapidly. Eventually, we reach the dim boundary - the utmost limits of our telescopes. There, we measure shadows, and we search among ghostly errors of measurement for landmarks that are scarcely more substantial. The search will continue. Not until the empirical resources are exhausted, need we pass on to the dreamy realms of speculation"

-Edwin P. Hubble

2.1 Importance of Bars

In the early parts of the twentieth century it was anticipated that *barred galaxies* would present an important niche in the study of "extragalactic nebulae". Heber D. Curtis (1918a) made the observation that,

> "*there is one fairly common type of spiral... Its main characteristic is a band of matter extending diametrically across the nucleus and inner parts of the spiral. Frequently the whorls in this type form a nearly complete ring; in other examples the whorls appear to begin at the ends of this cross-arm. The general appearance is that of the Greek letter* ϕ."

Less clear was the rôle that bars would come to play in the next century. Curtis (1918b) goes on to say, in "A Study of the Occulting Matter in the Spiral Nebulae",

> *"... the occurrence of such dark bands in the spiral nebulae is a relatively common phenomenon. This fact can scarcely fail to be of great importance in the study of this highly interesting and still imperfectly understood class of celestial objects."*

It is now these "*imperfectly understood celestial objects*" to which we turn the attention of this dissertation.

By definition barred galaxies comprise bulges, disks, lenses, rings, and of course, bars themselves (Sandage 1961; de Vaucouleurs 1959; Kormendy 1979; Sellwood & Wilkinson 1993; Buta 1995; Buta & Combes 1996). Bars are one of the most common morphological features of, and the most important internal perturbations in, disk galaxies. A bar is an elongated mass often made of old stars crossing the center. If spiral structure is present, the arms usually begin near the ends of the bar. Although most easily recognized in the face-on view, bars have generated great interest recently in the unique ways they can also be detected in the edge-on view. Not all bars are made exclusively of old stars. In some bulge-less galaxies, the bar has considerable gas and recent star formation.

Bars contribute to about 30% of a galaxy's total luminosity (Binney & Tremaine 1987), and often dominate the surface brightness distribution in the inner regions. They are also predominantly composed of the older Population I stars, and are thus dynamically important. The definition of Population I and Population II components has historically been rather broad. Since the 1957 Vatican Conference however, usage of "old Population I" has generally been confined to disk stars with high metallicity, while "Population II" now refers to the low metallicity halo population. The *gaseous* Population I component contains HII regions, OB associations, dust and cold interstellar HI gas, which are active and dynamically responsive regions. These are typically characterized by small, random motions (i.e.: a "cool disk") and in turn fuel Jeans instability. In contrast, the Population I stellar backbone is dynamically "warmer" and contains the *older population*, which, together with a constant mass to light ratio assumption, reveals the underlying mass distribution (Lin 1971).

Elmegreen & Elmegreen (1985) recognized that bars come in two "flavors": "flat" bars with uniform intensities along their lengths, prevalent in early-type spirals, and exponential bars whose intensity decreases exponentially and reside in late types. Models by Combes & Elmegreen (1993) show that this could be attributed to the location

of corotation which, because of the larger bulge-to-disk mass ratio in early-type disk galaxies, is closer to the nucleus and enables a more efficient growth of the bar and angular momentum transfer.

The phenomenon of bars in disk galaxies implies non-axisymmetric gravitational fields. Non-axisymmetric features are a pervasive and complex aspect of disk galaxies and their presence in galactic disks impact the evolution of morphology, such as inducing large-scale streaming motions in the stars and the gas (Athanassoula 1992a; Piner et al. 1995; Teuben 1995). Unlike stars, the gas in the galaxy is more collisional and dissipative, losing angular momentum and flowing inward down the bar dust lanes (Combes & Gerin 1985; Athanassoula 1992b; Regan et al. 1997, 1999; Sheth et al. 2000, 2002, 2005). This inward flow leads to striking changes in the host galaxy such as accumulation of molecular gas in the central nuclear region (Sakamoto et al. 1999; Sheth et al. 2005), smoothing of the chemical abundance gradient (Martin & Roy 1994), leading to circumnuclear star formation (Ho et al. 1997a, 1997b) and possibly the formation of bulges and pseudobulges (Norman et al. 1996; Kormendy & Kennicutt 2004; Sheth et al. 2005). Bars may drive spiral density waves (Kormendy & Norman 1979), generate resonance rings of gas (Schwarz 1981; Buta & Combes 1996), fuel active galactic nuclei (Shlosman et al. 1989), or induce gas inflow that may lead to bar destruction and bulge growth (Norman, Sellwood & Hasan 1996; Das et al. 2003). A spiral may trigger shocks, inducing star formation (Roberts, Roberts, & Shu 1975), or may rearrange star-forming regions into a more organized pattern (McCall 1986). To understand the evolution of spiral galaxies it is essential to understand the bar fraction and bar properties.

2.2 The Bar life-cycle

The distribution of bar strengths in disk galaxies is a potentially powerful way of studying galaxy evolution, and in particular the origin and evolution of bars themselves (Sellwood 2000). Bars in spiral galaxies with a normal gas content are transient features, because of the effects of growing central mass concentrations, gravitational torques, and decoupled nuclear bars. Bournaud & Combes (2004) present a detailed study of bar dissolution mechanisms, and argue that bars cannot be long-lived, except in gas-poor spiral galaxies. With physical parameters of normal spiral galaxies, these authors find that the bar life-time is 1 to 4 Gyrs, and may have been even less in the past. This

implies that the large fraction of barred galaxies observed today insists that bars are indeed transient. Furthermore they discuss the reformation mechanisms of bars, and show that the most efficient one is the accretion of large amounts of gas by spiral galaxies which reforms bars, maintains spiral arms, and may even explain warps, thick disks, and lopsidedness.

Several Gyrs ago, the velocity dispersion of gas in galactic disks was much higher. Forster-Schreiber (2009) find velocity dispersion at $z \sim 2$, to be typically $30 - 90 km/s$ at a time when galaxies were forming their thick disks, unlike the $10 km/s$ seen today. These thick disks survive only as remnants in nearby galaxies, very faint compared to the main disks. It is unclear whether bars could have formed at such an early epoch since bars presumably cannot form as easily in a hot disk as in a cool disk and as such it is likely to have taken some time for a disk to cool before bars could be formed. Observationally, bars at high redshift can easily be missed because the NIR light in which they are unveiled from dust is shifted to longer wavelengths. Accounting for this effect, Sheth et al. (2003) have reported that bars are common at redshift $z > 0.6$. They even find that these bars can be long compared to the disk radius, i.e.: with a high axis ratio. Bars were already present in spiral disks several Gyrs ago may suggest that they are long-lived features (Miller 1996). An alternative scenario is that bars are dissolved and reformed (Sellwood 1996). It is then fundamental to know whether bars are robust or short-lived.

Gas in barred galaxies is concentrated on the leading edge of the bar (de Vaucouleurs & de Vaucouleurs 1963). This is reproduced in single particle hydrodynamical simulations (Athanassoula 1992), as well as in the sticky-particle models of Bournaud & Combes (2004) which uses the hydrodynamical code of Junqueira & Combes (1996). The dissolution of bars is usually attributed to the growth of central mass concentrations (CMCs). The bars themselves, through their gravitational torques, fuel these concentrations over a few dynamical times. The growth of a CMC, through a process of dissipating orbits (Pfenniger & Norman 1990), can strongly weaken the bar. Shen & Sellwood (2004) discuss dissolution of bars with CMC masses of 0.5 to 2% of the disk mass. However, these authors also claim that bars are robust compared with the specific growth of CMCs. They find that realistic CMCs are not massive and/or concentrated enough to fully dissolve bars but only to partially weaken them.

A bar is destroyed by two main mechanisms: first, the central mass concentration built after gas inflow destroys the orbital structure sustaining the bar, scatters parti-

cles and pushes them on chaotic orbits (Hasan et al. 1990, 1993, Hozumi & Hernquist 1999). Secondly, the complete dissolution of a bar is not an effect of a CMC alone, but is triggered by the presence of gas. Indeed, bars are not dissolved in purely stellar simulations (Bournaud & Combes 2004). Growth of CMCs are not the only effects of gas; gas also exerts gravitational torques. These authors measure gravitational torques in simulations, with and without gas, to determine their impact on weakening bars and conclude that gravitational torques exerted by gas can fully dissolve bars far more efficiently than CMC growth. Here the torques due to the stellar backbone contribution tend to make orbits more circular. Furthermore the gravitational torques are responsible for about 15% of gas angular momentum loss in one rotation. The gas mass is only 5 to 10% of the stellar mass, and so torques exerted by gas on the Population I component stars will make them increase their angular momentum by about 1% per rotation. The gravitational torques exerted by gas will therefore dissolve the bar, in 10 to 20 rotations.

A third process is responsible for bar weakening in early-type spirals. These galaxies have bars with Inner Lindblad Resonances (ILRs) in which kinematically cold disks are observed. The properties of these cold disks can be matched in simulations of bar-driven gas inflows (Wozniak et al. 2003). Nuclear arms and bars are observed in these nuclear disks (Emsellem et al. 2003), and are also reproduced in numerical simulations. The pattern speed of the nuclear bar is different from the pattern speed of the main bar. This means that orbits inside the ILR leave the main bar alignment, which is likely to weaken the bar. Moreover, a nuclear bar may initiate a nuclear gas infall, which makes the mass more concentrated than without a nuclear bar.

Finally, the bar life-time rarely exceeds 4 Gyrs, except in unusually gas poor spiral galaxies (<4% of gas in their disk), and massive bulges. In *these* galaxies, bars can last a Hubble Time. It is believed galaxies were more gas-rich and disk-dominated a few Gyrs ago. Gravitational torques were consequently higher, and could fuel more massive central concentrations. We therefore expect bars at intermediate and high redshift to be shorter-lived than today. The bars observed at redshifts larger than $z = 0.6$ cannot have lasted for more than a few Gyrs in such gas-rich galaxies.

The ubiquity of bars in gas rich galaxies today then implies that they have been reformed after their dissolution, or that an external process has prevented their dissolution. Elmegreen et al. (2009) find that the bar in the strongly barred archetype NGC 1365 is 1- 2 Gyr old. Two mechanisms may reform bars: (1) galaxy interactions

and (2) accretion of large amounts of gas (Sellwood 1996). Berentzen et al. (2004) have shown that interactions can trigger bars in gas-poor galaxies, but cannot reform bars that have been dissolved in galaxies that harbor modest quantities of gas. Thus, interactions have only limited effects on bars at $z = 0$, and were even less efficient in reforming bars a few Gyrs ago, when galaxies were more gas-rich. Simulations support this prediction: galaxy interactions are not efficient enough to explain the ubiquity of bars in the local universe. This scenario of bar reformation through gas accretion is in good agreement with observations. Simulations by Bournaud & Combes (2004) are able to reproduce the distribution of bar strength observed in the local universe (Block et al. 2002, Buta et al. 2004), provided the gas accretion rate on spiral galaxies is of the order of 10 $M_{\odot}.yr^{-1}$. Such an accretion rate between $z = 0$ and $z = 1$ is expected from cosmological models (Semelin & Combes 2002). Gas accretion on spiral galaxies not only reforms bars, but also maintains spiral arms. Bars also change their pattern speed when they are reformed. Finally, spiral galaxies are open systems. Their Hubble type can change in a few dynamical times. Inner mechanisms tend to make them evolve toward earlier-types, but external gas accretion compensates for these effects and thereby drives late-type classes (Figure 2.1, Bournaud & Combes 2004).

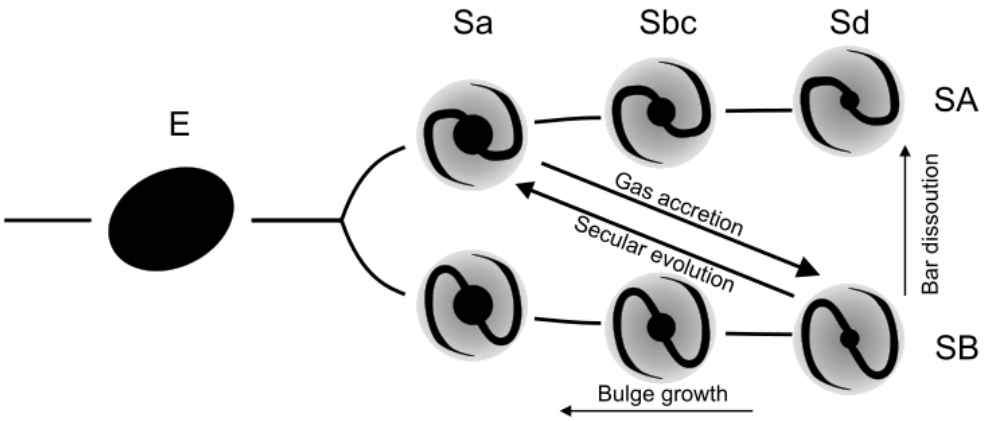

Figure 2.1: The bar dissolution/rejuvenation cycle: Interplay between gas accretion and secular evolution. External gas accretion drives the formation of bars, moving galaxies towards the lower-right. Secular evolution dissipates bars, and tends to evolve galaxies to upper-left. (Bournaud & Combes 2004).

An accurate measurement of the bar fraction depends on a variety of selection biases such as surface brightness limits, signal to noise ratio (S/N), inclination, and spatial resolution (Sheth et al. 2003, 2004). The bar fraction measurement is particularly sen-

sitive to the spatial resolution of the data. For instance, Sheth et al. (2003) show how the bar fraction measured in the Hubble Deep Field North using the coarse NICMOS data is comparable to the local Third Reference Catalog of Bright Galaxies (de Vaucouleurs et. al, 1991), hereafter RC3, fraction when the bar size is taken into account. A number of studies have looked at the bar size distribution of optically selected (i.e., RC3 SB/SAB) nearby barred galaxies (Kormendy 1979; Elmegreen & Elmegreen 1985; Martin 1995; Erwin 2005). These optical studies have found that bars in early-type spirals tend to be longer than those found in late types.

Using blue sensitive photographic plates, de Vaucouleurs (1963) found that 35% of all nearby spirals (S0/a to Sd) are strongly barred (SB) and 29% are "intermediately" barred (SAB). Eskridge et al. (2000) and Whyte et al. (2002) used 186 & 113 H-band images, respectively, of nearby galaxies classifying 75% of them as barred. Eskridge et al. (2000) identified bars using visual inspection (e.g., RC3), while Whyte et al. (2002) used a quantitative method to identify bars based on the method described by Abraham et al. (1996). In this dissertation bars are identified using the quantitative method described by Combes & Sanders (1981) for galaxies imaged at $3.6\mu m$ and $4.5\mu m$, as well as by fitting Isophotal Ellipses on deprojected images of galaxies at $3.6\mu m$.

2.3 Morphological importance of Dust in Barred galaxies

The subject of dark nebulae and what makes them dark have been favorite subjects of controversy since before the 20th century, culminating in the famous Shapley-Curtis debate (Shapley & Curtis, 1921). Curtis' argument is stated succinctly in Publications of the Lick Observatory (Curtis, 1918c), where he asserts, "*It has long been a matter of common knowledge that certain spiral nebulae seen edgewise show a dark lane running down the length of the spiral, an appearance generally explained as due to a band of absorbing or occulting matter.*" A matter of common knowledge even to Slipher (1917), who observed "*It is well known that spiral nebulae presenting their edge to us are commonly crossed by a dark band.*" He goes on (correctly) to surmise "*It doubtless has its origin in dark or deficiently illuminated matter on our edge of the nebula.*" and that "*if we view such a nebula from a point outside its plane the dark band would shift to the side and render the nebula unsymmetrical - the deficient edge being of course the one nearer us.*" Implicit in Slipher's method of determining the near-side of a galaxy

by simply looking at its "dark band" morphology, is the assumption that the "dark bands" were indeed made of occulting matter. Shapley, on the other hand, maintained he found no evidence of such obscuring matter, particularly in his observations of globular clusters - an argument which turned out to be irrelevant because the globular clusters he observed are outside the plane of the galaxy. The mysterious occulting matter is confined to the so-called "plane of avoidance", i.e.: the galactic plane. There was some sort of selection bias at work.

Trumpler (1930) presented conclusive evidence for the nature of this bias by comparing the luminosities and distances of open clusters. He thereby produced a reddening curve by knowing the spectral distribution of stars and compared their color excess with increasing distance. His observations furthermore revealed reddening even where no "clouds" were observed. By 1939, Stebbins, Huffer & Whitford observations evinced a λ^{-1} "law" of reddening. Whitford (1948) published measurements of star colors versus spectral types over a wavelength range from the ultraviolet to the near infrared. The relation was not the expected straight line, but showed curvature at the near ultraviolet and infrared regions. These phenomena could be explained from the point of view of small particle scattering. Van de Hulst (1949) calculated the temperature of these "small particles" whose absorption characteristics are highly dependent upon their physical size - absorbing energy well at short optical wavelengths, but poorly at longer ones.

We now know interstellar grains of dust in spiral galaxies comprise a dynamic range of sizes. Typically dust grains are so small they resemble the constituency of smoke, being anything from true macro-molecules up to $10\mu m$ in size (Greenberg & Li 1996). It is these particles which are responsible for dust extinction and reddening in galaxies. Interstellar light traversing through a galaxy encounters these tiny dust grains and those whose wavelengths are shorter than the physical size of the dust grains are preferentially absorbed. The longer, redder wavelengths are far less affected and when the radiation wavelength approaches the near-infrared regime the attenuation due to scattering is less than 10% that of the optical passband at V-band (Rieke & Lebofski 1985). The chemical constituents of these dust grains comprises silicates, ices and carbonaceous material. One of the most ubiquitous types of macromolecules proposed for tiny interstellar grains are polycyclic aromatic hydrocarbons (PAH). The variation in the relative proportions of these different constituents is one of the most important characteristics of interstellar cosmic dust and the spectral properties of cosmic dust in infrared emission provides a

method of determining the size distribution of the dust particles as well as the typical intensity of the starlight to which the dust is exposed. Consequently, the total dust mass can be calculated (Draine & Li 2007).

The optical depths inferred from dust grain extinction can be quite misleading, since not all scattered starlight by dust implies a loss in surface brightness of a galaxy. Extinction by dust grains is due to absorption as well as scattering. The presence of a relatively high dust mass fraction does not necessarily imply a large decrease in the surface brightness profile, because scattering may fill in some of the intensity lost due to absorption. Indeed, Disney et al. (1989) argue that the extinction due to dust based upon optical thickness, is highly model dependent, based on dust distribution models discussed by Valentijn (1990). Witt et al. (1992), show that scattering in the radiative transfer process introduces a bluing effect. With sufficient amounts of dust, this bluing can result in almost neutral broad-band photometric colors. Surface scattering off the dust may also attribute to an increase in the otherwise expected loss of apparent luminosity, as is the case with the reflection nebula discernible in NGC2841 as an amorphous linear strip transverse to the nearside minor axis (Block et al., 1999). The nebula exhibits an identical spectrum to that of the bulge light, and is typical of late type stars found primarily in the bulge. This has been attributed to the bulge light reflecting off a dense dust lane.

Interstellar dust grains are inexorably intertwined with galaxy morphology. In particular dust lanes in barred spirals are understood to be the loci of shocks. These occur on the leading edges of a bar where the velocity fields of gas and dust intersect and thereby experience an abrupt change in velocity, both in magnitude and direction. These shock fronts induce vast streams of galactic dust cascading down the gravitational potential towards the centers of galaxies. A well known prototype for this pattern is NGC1300, which is classified by Hubble as SBb(s).

The shape and spatial location of dust lanes in spiral galaxies have been modeled in a number of theoretical studies by focusing on the hydrodynamic response of gas and dust in disks, in close proximity to rotating bars. Prendergast (1962) pioneered hydrodynamic models including the phenomena of gas shocks in the neighbourhood of a bar. Early dust velocity field predictions are detailed in Huntley et al. (1978), which have subsequently been summarized by Prendergast (1983) for SBb and SBc galaxies. These were further investigated by Athanassoula (1984) who predicts two distinct dust lane morphologies: (i) straight lanes, and (ii) concave curved lanes, where the concave

side is towards the bar major axis. In these models, the dust lanes appear on the leading edges of bars as defined by a trailing set of spiral arms. Athanassoula (1992b) presents comprehensive simulations showing the degree of curvature of dust lanes coincides with optical bar strengths. Ann and Lee (2000) performed smoothed particle hydrodynamics (SPH) simulations of the evolution of gaseous disks and present gas morphologies of a range of synthetic barred galaxies. Ann (2001) further investigates the formation of nuclear gas and dust rings by making extensive use of SPH simulations. Comerón et al. (2009), using a sample of 55 nearby barred spiral galaxies, observationally verify that strong bars (high Q_g) imply dust lanes with low curvature, whereas weak bars could harbour dust lanes with a wide range of curvature. Thus very straight dust lanes are expected where there is a rapid change in direction for the gas and dust velocity field at the outermost orbits where they cross the bar long axis. Athanassoula investigates various apo-centre curvatures using van Albada's (1981) second-order flux-splitting models and predicts that strong bars produce relatively straight dust lanes. The gas and dust density, along with the velocity field vectors are seen in Athanassoula (1992). The presence of flocculent spurs emanating from the gas and dust lanes at the shock positions reveal a well ordered, intricate velocity field along the shock loci.

As regards gas and dust transport, in cases where no shocks are evident there is no net inflow towards the nucleus. However, in cases with shocks the trailing sides of the bar exhibits gas outflow where the gas density is very low (Piner et al. 1995). This outflow continues until it reaches the shock front, where it abruptly turns inward and results in the formation of dust lanes. Since dust lanes are understood to be regions of higher gas density and dust concentrations, one might conclude that this should influence the local star formation rate. The reason star formation is not prevalent at all is attributed to the high shear encountered in straight dust lanes. Molecular clouds will thus tend to shear out before they have time to collapse, preventing any star formation in that region. Dust lanes with a higher degree of curvature, however, may well harbor more benign environments for incipient star formation. These processes would thereby drive the morphology of barred spirals and influence their position along their evolutionary continuum (Figure 2.1).

2.4 Bars in the near infrared

Bars are fundamental components in the distribution of mass in galaxies due to the fact that they principally consist of an old stellar population (de Vaucouleurs 1955; de Vaucouleurs & de Vaucouleurs 1959; Freeman 1989; Elmegreen & Elmegreen 1985). Bars are believed to induce a wide variety of secular evolution processes in galaxy dynamics (Pfenniger, Martinet, & Combes 1996) which leads to significant changes in galaxy structure over a Hubble time. Disk galaxies, as star producing systems, must contain a lot of gas. The effects of this gas needs to be considered over a Hubble time. Dust polluted gas is very efficient in losing thermal energy by infrared radiation, implying that galaxies also need to be considered as energy dissipating structures. Gravitationally bound rotating structures rapidly converge towards thin disks because angular momentum is far more resistant to dissipation than compared with thermal energy.

The relevance of observed wavelength to the detection of bars was first pointed out by Hackwell & Schweizer (1983) who discovered a strong bar in NGC 1566 at H-band. Previously undiscovered bars have been detected with the advent of large format near infrared arrays (Hackwell & Schweizer 1983; Scoville et al. 1988; Thronson et al. 1989; Mulchaey & Regan 1997; Seigar & James 1998; Jarrett et al. 2003). A rich duality of spiral structure has been found from studies of optical and near-infrared images. A spiral galaxy may present two completely different morphologies when examined optically and in the near-infrared (Elmegreen et al. 1999; Block et al. 1999; Eskridge et al. 2000). In the optical, dust often hides bars, as in the Milky Way whereas the near-infrared light comes principally from old giant and supergiant stars (Frogel et al. 1996) and the extinction at H and K-band is only 10%-20% times that in visual light, so that dust has only a minimal effect on the inferred potentials. Near-infrared H-band and K-band images beautifully reveal the old stellar population or "backbone" of spiral galaxies (Frogel, Quillen, & Pogge 1996; Block et al. 1994; Block et al. 1999).

Large format NIR cameras have come of age over the last two decades. These have been instrumental in examining the bar fraction in the optical and NIR between active and nonactive galaxies, to determine the rôle of bars in feeding active galactic nuclei (AGNs) (Mulchaey & Regan 1997; Knapen et al. 2000; Laine et al. 2002; Laurikainen et al. 2004). Laine et al. (2002) and Laurikainen et al. (2004) have compared properties of H-band selected bars in active and nonactive galaxies. Furthermore, the advent of

large, deep extragalactic surveys such as OSUBGS, COSMOS, GOODS, GEMS, SINGS and S^4G (Eskridge et al. 2002; Scoville et al. 2007; Dickinson et al. 2003; Rix et al. 2004; Kennicutt et al. 2003; Sheth et al. 2009) has triggered studies that explore the evolution of the bar fraction (Sheth et al. 2003, 2004; Elmegreen et al. 2004; Jogee et al. 2004).

Eskridge et al. (2002) use OSUBGS H-band images to classify NIR galaxies within the revised Hubble framework of de Vaucouleurs (1959) and Sandage & Bedke (1994). These H-band classifications, treated as if the images were blue-light images, were converted to the RC3 numerical T-type index. Eskridge et al. (2002) note that the apparently increased bulge-to-disk ratio and the greater degree of smoothness of structure biases these NIR classifications toward earlier types. From a bar fraction perspective, NIR classifications from the OSUBGS sample show approximately twice as many strongly barred (SB) disks as in the optical. The reason for this difference is attributed to NIR images accentuating weak bars more. Therefore, NIR imaging does not necessarily change the classification of bars much and there is no additional bin for a B-band SB spiral to be placed in, even though the bar looks stronger in the NIR. A B-band SAB spiral can however be "upgraded" into the SB category in the NIR. Further improvements can be made by obtaining two-dimensional velocity fields of the galaxies in this sample which would facilitate the derivation of kinematic orientation parameters and improved deprojection. There is a significant dependence of the maximum relative gravitational torque on the revised optical Hubble type. This effect is robust and persists when the sample is divided into bar-dominated and spiral-dominated types. Bars and spirals tend to have weaker average relative torques in early-type disks compared to that of late-type spirals. This is most likely due to torque-dilution of stronger bars due to the stronger bulges in early-type spirals.

Seventy percent of spirals classified in the Carnegie Atlas of Galaxies (Sandage & Bedke 1994), based on Hubble bins, are classified as unbarred. This fraction drops to 27% when these galaxies are imaged in the near-infrared (Eskridge & Frogel 1999). This means 73% show ovals or bars in the dust-penetrated regime. This high percentage of bars in the near-infrared agrees with the findings of Seigar & James (1998), who find that 90% of a sample of 45 galaxies showed some evidence of a bar in the K-band.

Menéndez-Delmestre et al. (2007) find a lower limit to the NIR bar fraction measured in a sample of 151 2MASS galaxies. The fraction of galaxies with bars in their sample is 67%. They identify 85% of all SB galaxies and 80% of all SAB galaxies from

the RC3 in their sample as barred spirals. In addition, these authors find 11 galaxies within the RC3 SA category to be barred spirals. This lower limit to the NIR bar fraction is conservative because it is restricted to barred galaxies which show a positive ellipticity and position angle signature. It is consistent with the bar fraction of 59% found by Laurikainen et al. (2004), who apply a Fourier decomposition method to a sample of 180 spirals with an inclination less than 65 degrees. Marinova & Jogee (2007) confirm this result with a measured local universe H-band bar fraction of 58%. These analyses compare well with the total fraction of 63% SB and SAB galaxies in the RC3 B-band analysis. While the relative fraction of weak (SAB) or strong bars (SB) shifts toward the NIR from optical passbands, the overall fraction of barred galaxies remains relatively unchanged throughout this spectral region. This indicates that strong-bar morphology can be reliably detected by eye at optical wavelengths.

2.5 Quantitative Measures of Bar Strength

Although the eye is excellent at discerning visual details, it is not an objective classification tool. Visual inspection of images is unreliable for poor-quality and low signal-to-noise (S/N) data, such as in the context of high-redshift galaxies. With increasing redshift there is a corresponding significant decline in the spatial resolution or decreased S/N. Classification by eye is also tedious for large data sets and is always subjective. In such cases an automated method for bar identification is more useful as it has the advantage of reproducibility and can easily be applied to large data sets. Moreover, an automated algorithm that uses the full two-dimensional light distribution is likely to be more robust than relying on the human retina.

Various quantitative measures of bar strength have been suggested in the literature. The bar-interbar contrast, developed by Elmegreen & Elmegreen (1985), can distinguish strong bars from weak bars. Sometimes the maximum bar-interbar contrast occurs inside the radius of the bar, but in some cases it may occur outside the ends of the bar, as in NGC 1433 (Buta 1986). Also, Seigar & James (1998) note that bar-interbar contrasts are sensitive to resolution and seeing effects. Elmegreen & Elmegreen (1985) derive relative bar luminosities in terms of m=2 and m=4 components using Fourier intensity amplitudes. Ohta, Masau, & Wakamatsu (1990) derive similar parameters for six barred galaxies, including the m=6 term.

A readily accessible measure of the strengths of bars is the deprojected bar ellipticity, ϵ_b, as developed by Martin (1995) and suggested by analytical models (Athanassoula 1992a). It is commonly used because of its simplicity and it being independent of spectroscopic observations, surface photometry, and mass-to-light ratio assumptions. Martin (1995) derived ϵ_b for more than 100 spiral galaxies by visual inspection of published optical photographs and noted that the slope of chemical abundance gradients (Martin & Roy 1994) as well as the presence of nuclear star formation (Martin & Friedli 1997) depend on ϵ_b. This parameter or its equivalent, $1-(b/a)_{bar}$, has also been used by other authors, such as Rozas, Knapen, & Beckman (1998); Aguerri (1999); Chapelon, Contini, & Davoust (1999); Abraham et al. (1999); Shlosman, Peletier, & Knapen (2000). Abraham et al. (1999) describe an algorithm that automatically derives $(b/a)_{bar}$ from moments of the galaxy images. When $(b/a)_{bar}$ is plotted against morphological T type, there is a trend for bar axial ratios to decrease with increasing Hubble type; earlier Hubble types tend to have "fatter" bars. This trend for bar axial ratios is similar in kind to the trend found by Buta et al. (2004) for maximum Q_g as a function of Hubble type. Thinner bars tend to be classified as SB, while fatter ones appear as SAB, or are completely elusive (SA).

Abraham & Merrifield (2000) describe a refinement on the bar axis ratio using a parameter f_{bar} defined as "the minimum fraction of the bar's stars that one would have to rearrange in order to transform the structure into an axisymmetric distribution". Seigar & James (1998) developed another quantitative approach to bar strength that utilizes near-infrared surface photometry. In their method, the bar is defined to be the light remaining after disk and bulge components are subtracted. This light is converted into a parameter known as "equivalent angle", which is defined to be "the angle subtended at the centre of the galaxy by a sector of the underlying disk and bulge that emits as much light as the bar component, within the same radial limits". Rozas et al. (1998) derived another flux parameter, σ_b, representing the ratio of the flux inside the bar to that outside the bar area. They argue that this parameter and ϵ_b indicate that stronger bars are accompanied by a lower degree of symmetry of star formation in the spiral arms. In each of these methods, the bar itself has to be defined, e.g., where it appears to start, where it appears to end, or where the maximum ellipticity is achieved.

Block & Puerari (1999) proposed a classification scheme involving near-infrared images to develop shear-related pitch angle classes. These classes are determined by the dominant Fourier harmonic in the spiral arm, which is the main classification parameter.

In this classification, a ubiquity of low-order ($m = 1, 2$) Fourier modes for both barred and unbarred galaxies are found in the near-infrared regime, consistent with the modal theory of spiral structure (Bertin & Lin 1996; Block et al. 1999). Galaxies with a dominant Fourier $m = 1$ mode are L(lopsided), while galaxies principally showing an $m = 2$ harmonic are E(evensided). Using the Fourier spectra, galaxies were binned into three different subclasses, α, β, & γ, based on the pitch angle of the spiral arms of approximately 10°, 25° and 40° respectively.

Our approach here is based instead on the torques induced by the rigidly rotating bar, without first having to accurately define and isolate it relative to the other components in a galaxy. Determination of the maximum force ratios for a large, statistically well defined sample of galaxies may provide us with a handle on some probing questions regarding bar formation scenarios (Sellwood 2000), such as bar instability (Miller, Prendergast, & Quirk 1970; Hohl 1971; Sellwood & Wilkinson 1993) or tidal bar formation (Noguchi 1996; Miwa & Noguchi 1998). Determining characteristic bar number frequency distributions of maximum relative bar torques thereby provides a distinguishing mechanism between these scenarios. For example, recurrent bar formation due to external gas accretion would impact the distribution of maximum force ratios (Bournaud & Combes 2002). The idea that bars can be the engines of their own destruction in the presence of gas is advocated by Das et al. (2003). Furthermore, incipient bar formation may occur if a galaxy accretes sufficient quantities of external gas during a Hubble time that will cool the disk (Sellwood & Moore 1999). Block et al. (2002) conclude that the distribution of maximum relative torques of the Ohio State University Bright Galaxy Survey (OSUBGS; Eskridge et al. 2002) favored galaxy gas accretion rates which typically double their mass in 10^{10} years.

2.6 Relative Gravitational Torques

Studies of maximum relative torques in spiral galaxies have centered around several issues: (1) quantitative dust-penetrated bar classification (Buta and Block 2001); (2) the distribution of these torques (Block et al. 2002; Buta, Laurikainen & Salo, 2004); (3) a comparison of torques between active and nonactive galaxies (Laurikainen, Salo & Rautiainen, 2004; Laurikainen, Salo & Buta, 2004); (4) the correlation between bar torque strength and inner ring shape (Buta 2002), and (5) the relation, if any, between maximum bar torques and spiral torques in the same galaxy (Buta, Block & Knapen,

2003a; Block et al. 2004).

Block et al. (2002) derived the distribution of Q_g values based on a preliminary analysis of OSUBGS H-band images of 163 galaxies. These authors did not account for bulge shape and used a fixed relation between the radial scalelength and the vertical scaleheight: $h_z = h_r/12$, which partly led to a deficiency of low Q_g values. Buta, Laurikainen & Salo (2004) used a more refined application of the GTM (Laurikainen, Salo & Buta 2004).

In principle, this is an excellent physical means of measuring bar strength. In practice, the method requires assumptions about disk structure that are difficult to verify. It also requires high spatial resolution, high S/N images, and is very laborious to implement. Application of the GTM involves several uncertainties which need to be carefully analyzed. The main assumptions are: (i) the NIR light distribution traces the mass distribution, i.e. a constant M/L is assumed, (ii) the vertical density distribution can be approximated by some simple functional form, like an exponential profile, with some proper scale parameter h_z. In the bar region where the maximum Q_g typically occurs, the effect of halos is generally insignificant for bright galaxies, as shown in Buta et al. (2004) by applying the correlation between galaxy luminosity and dark halo contribution found by Persic et al. (1996). The effect of unknown vertical structure is more problematic: although the exact functional form is not crucial (Laurikainen & Salo 2002), the derived Q_g depends significantly on the assumed vertical scale height. Buta et al. (2004) have tried to reduce this uncertainty by connecting h_z to the radial scale length h_r, using Hubble-type dependent empirical h_z/h_r ratios derived by de Grijs (1998). Typically, the uncertainty in h_z is $\pm 5\%$ for late type spirals, increasing to approximately $\pm 25\%$ for early type spirals (Laurikainen, Salo & Buta 2004).

The calculation of force ratios provides a straightforward method for characterization of perturbations associated with bars and spirals, provided that the vertical extent of the disk can be estimated. In particular, azimuthal smoothing implicit in the polar method makes the results fairly robust against image resolution and noise. This makes the method feasible also for intermediate and high redshifts, provided that disk orientation and scale length can be reliably estimated. Treatment of a spherical bulge helps to remove effects of artificial bulge stretch, but further improvements might still be needed in order to apply the method for systems with higher h_z, or to systems with triaxial bulges.

The methods examined here provide statistically self-consistent results, even when comparing different methods in different wave-bands (i.e. NIR torque methods compared with B-band bar ellipticity). Thus any of the methods discussed here can provide a good statistical means of measuring bar strength. This argues that bar-strength analysis of high-redshift galaxy samples can, at least in principle, be compared with analysis of nearby systems even when the observations are at different rest-frame wavelengths, and at very different spatial sampling. Nevertheless, even gravitational torques and non-axisymmetric perturbations may not be the final word on the strength of bars. Recent models by Regan & Teuben (2004) suggest that Q_g is degenerate with several bar characteristics that are involved with ring formation because gravitational potentials with vastly different bar orbit morphologies can have the same Q_g. These authors conclude that Q_g may not be a useful diagnostic of bar strength, and question the extent to which a bar will have an effect on galaxy evolution.

The gravitational potential of bars, i.e.: bar torques, are poorly recognized by the Hubble classification scheme. Prominent bars can have either small or large relative torques, depending on the relative mass of the bulge. If the bulge is small (as in late types), then a weak bar can have a strong gravitational torque compared to the axisymmetric radial component since the bulge contribution does not dilute the relative torque as much. However, bars that are long can also have strong torques since the ends of the bar are far from the bulge. Therefore, a simultaneous increase in relative bulge strength and bar length would oppose influences in changing the gravitational torque. The method is thus highly sensitive to the specifics of the luminous mass distribution. Variations in torque with bar type are also not obvious from morphology. If bars drive spirals, particularly in early Hubble types where the presence of a bar correlates well with grand design spiral structure (Elmegreen & Elmegreen 1989), they may produce strong arms in very short dynamical times. This seems true for both strong and weak bar torques alike, since even weak torques are sufficient to induce strong spiral arms. As a result, there is little sensitivity in spiral arm strength related to bar torques, aside from the known sensitivity of arm strength to the relative magnitude of the m=2 component of the dust penetrated older Population I stellar backbone (Elmegreen & Elmegreen 1985).

In the remaining chapters we present a detailed NIR gravitational torque analysis of a select sample of nearby barred spiral galaxies imaged with the Infrared Array Camera on board NASA's Spitzer Space Telescope (Fazio et al. 2004). We furthermore identify

bars and characterize their sizes and ellipticities with a widely used technique of fitting ellipses to the full two-dimensional light distribution of the spirals in our sample, for example Wozniak et al. (1991); Regan & Elmegreen (1997); Zheng et al. (2005); and Barazza et al. (2007) in the optical, and Knapen et al. (2000); Laine et al. (2002); Laurikainen et al. (2002); Sheth et al. (2000, 2002, 2003); and Marinova & Jogee (2007) in the NIR.

Chapter 3

Gravitational Torque Method

"There are two mistakes one can make along the road to truth...not going all the way, and not starting"

-Buddha

"Ideas are beginning points of all fortunes."

-Napoleon Hill

3.1 Introduction

Non-axisymmetric features, with their associated pattern speeds and resonances, are extremely important in galactic evolution. Understanding how these features develop is one of the principal problems in galaxy formation scenarios. Sanders & Tubbs (1980) and Combes & Sanders (1981) suggested that tangential and axisymmetric radial forces would provide a quantitative measure of the strengths of non-axisymmetric features, with emphasis on bars, if the potential could be determined. Near-infrared images feature the older, dominant stellar population and as such, provide an adequate tracer of the stellar mass distribution and hence serve as an adequate source from which gravitational potential can be inferred. Fast Fourier transform techniques allow such potentials to be derived from these images, together with a constant mass-to-light ratio assumption and estimates of the vertical density distribution (Quillen, Frogel, & Gonzalez 1994). This potential provides the radial and tangential components of the forces in the plane of the galaxy, which, when expressed as a ratio, provides a single quantitative parameter describing the strength of the bar. Buta & Block (2001), Block et al. (2001, 2002), Laurikainen, Salo & Rautiainen (2002), and Laurikainen & Salo (2002) have paved the way to derive the maximum force ratios from various near-infrared nearby galaxy surveys. In this dissertation we examine the distribution

of maximum relative torques in spiral galaxies based on the application of the GTM to a sample of 40 Spitzer IRAC galaxies at $3.6\mu m$ and $4.5\mu m$. Our goal is to determine the impact of using $3.6\mu m$ and $4.5\mu m$ images of the same galaxies to understand the nature of stellar emission morphology at these wavelengths.

Several methods are available in order to measure bar strengths, for example, visual estimates of the bar strengths (Martin 1995; Eskridge et al. 2000, 2002), bar/interbar contrast, Fourier decomposition techniques (Elmegreen & Elmegreen 1985; Elmegreen et al. 1996), the maximum ellipticity of bars (Menéndez-Delmestre et al. 2007) and the gravitational torque method or most commonly known as the Q_b method (Block et al. 2002; Buta et al. 2003a, 2005).

3.2 Getting the Potential

Much of the galaxy's luminous mass distribution resides in stars. The gravitational potential of a collection of stars, such as a galaxy, can be calculated by simply adding the point mass potentials of all the stars in the ensemble. This approach however, is not practical for *all* the stars in a typical galaxy ($\approx 10^{11}$). To obtain the gravitational potential of a galaxy, an $n \times n$ array of cells is superposed over the galactic disk. The gravitational potential at the centre of the cell is then defined by:

$$\Phi_{x,y} = \sum_{i=0}^{N-1} \sum_{j=0}^{N-1} \mu_{i,j} H_{x-i,y-j} \tag{3.1}$$

where

$$H_{i,j} = \frac{1}{\sqrt{i^2 + j^2}} \quad \text{for} \quad i + j \neq 0$$
$$H_{0,0} = 1$$

and $\mu_{i,j}$ is the mass density in cell (i, j). $N = 2n$ defines the larger array over which the Fourier transform must be taken in order to obtain the potential of a galaxy. Hohl & Hockney (1969) calculated gravitational potentials of synthetic galaxies. Here they

evaluated the double summation in (3.1) by the convolution method using Fast Fourier transforms, i.e the Fourier transforms of the potential is equal to the product of Fourier transforms of μ and H

$$\tilde{\Phi}_{k,l} = \tilde{\mu}_{k,l}\tilde{H}_{k,l} \tag{3.2}$$

The gravitational potential $\Phi_{x,y}$ is obtained by taking the inverse Fourier transform of (3.2).

$$\Phi_{x,y} = \frac{1}{N^2}\left[\sum_{l=0}^{n}\left\{\sum_{k=0}^{n}\tilde{\Phi}_{k,l}\cos\left(\frac{\pi}{n}kx\right) + \sum_{k=n+1}^{N-1}\tilde{\Phi}_{k,l}\sin\left(\frac{\pi}{n}(k-n)x\right)\right\} \times \cos\left(\frac{\pi}{n}ly\right) + \sum_{l=n+1}^{N-1}\left\{\sum_{k=0}^{n}\tilde{\Phi}_{k,l}\cos\left(\frac{\pi}{n}kx\right) + \sum_{k=n+1}^{N-1}\tilde{\Phi}_{k,l}\sin\left(\frac{\pi}{n}(k-n)x\right)\right\} \times \sin\left(\frac{\pi}{n}(l-n)y\right)\right] \tag{3.3}$$

The Fourier transform techniques are applied using the Cooley & Tukey (1965) algorithm for Fast Fourier Transforms. This algorithm provides a more efficient way of evaluating the double sum in (3.1). The matrix $H_{k,l}$ only needs to be calculated for the first time step, thus at each time step the work done is given by $2[4klog_2(2k)]^2$ multiplications and additions to evaluate the two two-dimensional transforms and further $(2k)^2$ multiplications for the convolution. Using the fast fourier transforms all the $\Phi_{k,l}$ can be obtained in $(2k)^2[1 + 4log_2(2k)]^2$ arithmetic operations, which is more efficient compared to direct evaluations of the double sum which takes k^4 arithmetic operations.

3.3 Calculating Force Ratios

Using this gravitational potential $\Phi(R, \psi)$ of the disk plane, Combes & Sanders (1981) defined a quantitative parameter that can be used to classify models of galaxies according to their gravitational torques. These authors described this quantitative parameter "$Q_T(R)$" ($\equiv Q_g$) as a ratio of maximum tangential force to that of the axisymmetric radial force:

$$Q_T(R) = \frac{(\frac{\partial \Phi}{\partial \psi})_{max}}{R\frac{\partial \Phi_0}{\partial R}} \tag{3.4}$$

The availability of near infrared detectors in the early 1990's made it possible to quantitatively classify galaxies. The theory described by Hohl & Hockney (1969) to measure the gravitational potential, and gravitational torque parameter by Combes & Sanders (1981), was applied to J, H, and K band images of NGC 4314 by Quillen, Frogel & González (1994). These authors provided an efficient procedure for mapping the gravitational potential of a galaxy based on its appearance in the near infrared using the Fast Fourier Transform method.

Applying the algorithm described by Quillen, Frogel & González(1994) to a set of 36 William Herschel Telescope (WHT) images, Buta & Block (2001) describe a full continuum of bar strengths. Their parameter Q_g for bar strength depends on the actual forcing due to the bar embedded in its disk. In here they find a wide range of true bar strengths characterizing the category "SB", with a narrower range for the de Vaucouleurs category "SAB". They describe bar strength at radius R as given by Combes & Sanders:

$$Q_T(R) = \frac{F_T^{max}(R)}{< F_R(R) >} \tag{3.5}$$

where

$$F_T^{max}(R) = [\frac{\partial \Phi(R,\psi)}{\partial \psi}]_{max} \tag{3.6}$$

is the maximum amplitude in the tangential force at radius R and

$$< F_R(R) >= R(\frac{d\Phi_0}{dR}) \tag{3.7}$$

defines the mean axisymmetric radial force at the same radius, given by the $m = 0$ gravitational potential Fourier component. The maximum value of Q_T ($\equiv Q_g$) provides

a single measure of bar strength. The different classes of bar strength described by Buta & Block are provided in Table 3.1.

Q_g **Range**	<0.05	0.05-0.14	0.15-0.24	0.25-0.34	0.35-0.44	0.45-0.54	0.55-0.64	>0.65
Class	0	1	2	3	4	5	6	7

Table 3.1: Bar strength classes defined by Buta & Block (2001)

Their bar classes are based on measured values of Q_g: each class spans a range of 0.1 centered on a 10 percentile. For example: class 1 spans $Q_g = 0.1 \pm 0.05$ and class 2 spans $Q_g = 0.2 \pm 0.05$ etc., except for class 0 as it involves a narrower range of Q_g. The classes are described as follows: bar class 0 galaxies are the normal spirals without any bar, bar classes 1 and 2 consist of galaxies with weak bars and ovals i.e., de Vaucouleurs' SAB Class, and class 3-7 encompasses all galaxies that are of Hubble's and de Vaucouleurs' SB types. This method provides a full quantitative measure of bar strengths for spiral galaxies.

3.4 The Sample

Analyses with the GTM were performed on selected sample of 40 images of nearby barred spirals from both the IRAC $3.6\mu m$ and $4.5\mu m$ channels. These Spitzer data were retrieved from the Spitzer Heritage Archive at the Infrared Science Archive (IRSA) at the Infrared Processing and Analysis Center (IPAC), California Institute of Technology. Of these 40 galaxies, 8 are SAB galaxies, 1 is a SA galaxy and 31 are SB galaxies as described in de Vaucouleurs et al. (1991). The sample galaxies have distances $< 42Mpc$ and inclination $< 67°$ (RC3). 21 of the galaxies have a plate scale of $0.60arcsec/pix$, 13 with $1.22arcsec/pix$ and 6 with $0.75arcsec/pix$. All galaxies were assumed to have a scale height of 325pc, converted to h_z(arcsec) at their respective distances. These parameters, together with the distances and inclinations, can be found in Table 3.2.

Table 3.2: Properties of the GTM Sample (h_z = vertical scale height, T&F = Tully & Fisher 1987;T = Tully 1988)

Galaxy	**Type** (RC3)	$logR_{25}$	**Incl.** (degrees)	**Dist.** (Mpc)	**Source**	h_z (arcsec)	**Plate Scale** (arcsec/pix)
NGC0289	SB(rs)bc	0.15	44.93	19.4	T&F	3.46	0.60
NGC0600	(R')SB(rs)d	0.07	31.66	22.9	T&F	2.93	0.75
NGC0613	SB(rs)bc	0.12	40.66	17.46	T&F	3.84	0.60
NGC0685	SAB(r)c	0.05	26.97	15.2	T	4.41	1.22
NGC0936	$SB0^+$(rs)	0.06	29.43	16.9	T	3.97	1.22
NGC0986	SB(rs)ab	0.12	40.66	23.2	T&F	2.89	1.22
NGC1300	SB(rs)bc	0.18	48.65	18.8	T&F	3.57	1.22
NGC1326	(R)$SB0^+$(r)	0.13	42.16	16.9	T&F	3.97	1.22
NGC1365	SB(s)b	0.26	56.66	16.9	T&F	3.97	0.60
NGC1398	(R')SB(r)ab	0.12	40.66	16.1	T&F	4.16	1.22
NGC1433	(R')SB(r)ab	0.04	24.21	11.6	T&F	5.78	1.22
NGC1493	SB(r)cd	0.03	21.05	11.3	T&F	5.93	1.22
MGC1512	SB(r)a	0.2	50.88	11.6	T&F	5.78	0.60
NGC3198	SB(rs)c	0.41	67.10	10.8	T&F	6.21	0.60
NGC3319	SB(rs)cd	0.26	56.66	11.5	T&F	5.83	1.22
NGC3368	SAB(rs)ab	0.16	46.22	8.1	T&F	8.28	0.60
NGC3504	(R)SAB(s)ab	0.11	39.08	26.50	T	2.53	0.60
NGC3513	SB(rs)c	0.1	37.41	17	T&F	3.94	0.75
NGC3627	SAB(s)b	0.33	62.11	6.6	T&F	10.16	0.60
NGC3892	$SB0^+$(rs)	0.12	40.66	27.2	T	2.46	0.75
NGC4245	SB(r)0/a:	0.12	40.66	9.7	T	6.91	1.22
NGC4394	(R)SB(r)b	0.05	26.97	16.8	T&F	3.99	1.22
NGC4421	SB(s)0/a	0.12	40.66	16.8	T&F	3.99	0.60
NGC4450	SA(s)ab	0.13	42.16	16.8	T&F	3.99	0.60
NGC4535	SAB(s)c	0.15	44.93	16.8	T&F	3.99	0.60
NGC4548	SB(rs)b	0.10	37.41	0.18	T&F	3.99	1.22
NGC4593	(R)SB(rs)b	0.13	42.16	39.45	T&F	1.70	0.60
NGC4596	$SB0^+$(r)	0.13	42.16	16.8	T&F	0.39	0.75
NGC5101	(R)SB(rs)0/a	0.07	31.66	27.42	T&F	2.45	0.60

Continued on next page

Table 3.2 – continued from previous page

Galaxy	**Type** (RC3)	$logR_{25}$	**Incl.** (degrees)	**Dist.** (Mpc)	**Source**	h_z (arcsec)	**Plate Scale** (arcsec/pix)
NGC5371	SAB(rs)bc	0.1	37.41	37.8	T&F	1.77	0.60
NGC5375	SB(r)ab	0.07	31.66	37.8	T&F	1.77	0.75
NGC5383	(R')SB(rs)b:pec	0.07	31.66	37.8	T&F	1.77	0.60
NGC5921	SB(r)bc	0.09	35.63	25.2	T&F	2.66	0.75
NGC6217	(R)SB(rs)bc	0.08	33.72	23.9	T&F	2.81	0.60
NGC6744	SAB(r)bc	0.19	49.79	10.4	T&F	6.45	0.60
NGC7329	SB(r)b	0.17	47.46	42.12	T&F	1.59	0.60
NGC7479	SB(s)c	0.12	40.66	29.1	T&F	2.30	0.60
NGC7552	(R')SB(s)ab	0.10	37.41	19.5	T&F	3.44	1.22
NGC7741	SB(S)cd	0.17	47.46	12.3	T&F	5.45	0.60
IC1438	(R')SAB(rs)a	0.07	31.66	33.8	T&F	1.98	0.60

Images at these wavelengths trace the older Population I stellar backbone of disk galaxies as they image the Rayleigh-Jeans limit of the blackbody emission for stars with T > 2000K, and also do not suffer from excessive attenuation due to dust (Draine & Lee 1984). In nearby galaxies, the mid-infrared color is nearly constant with radius, and independent of the stellar mass distribution (Pahre et al. 2004). Hence these images are suitable for the analysis of bar strength. There is a weak $3.3\mu m$ PAH (Polycyclic Aromatic Hydrocarbon) feature in the $3.6\mu m$ band, which contributes $< 2\%$ to the overall emission in the band (Tokunaga et al. 1991). Near active galactic nuclei or extreme starbursts may experience emission contributions from small grains of hot dust ($T_d > 500$K). The effects of the $3.3\mu m$ PAH or hot dust emission have been deemed negligible on the sample of bright barred galaxies used in this dissertation. Analysis on these images were performed using IRAF and the gravitational potential code from Quillen, Frogel & González (1994), here after QFG. There are several steps that are required to prepare the images for analysis.

3.5 Preprocessing

The initial steps in preparing the images for analysis are to align and clean the images of any foreground stars. Aligning the images is achieved by obtaining the centers of galaxies using the IRAF routine IMEXAM and using these values as input parameters in IMLINTRAN (Figure 3.1(b)). Foreground stars are removed by replacing them with average background using a circular aperture (Figure 3.1(c)). In order to calculate the potential, QFG requires that all input images be square, with an array dimension of 2^n, where n is an integer. Images used were all resized to 512×512 when deprojecting the images. Deprojecting images requires several parameters, such as position angle, logarithmic axis ratio and the magnification factor. The values of position angle and logarithmic axis ratio can be obtained from the RC3. These values can then be used to deproject images using the IRAF routine IMLINTRAN (Figure 3.1(d)). Once the deprojection of all the images is accomplished, we need to rotate the images such that the bar of the galaxy is horizontal. This can be done using the IRAF routine ROTATE(See Figure 3.2). Images are now ready to go through the GTM process. For more details on these pre-processes, refer to Appendix A.

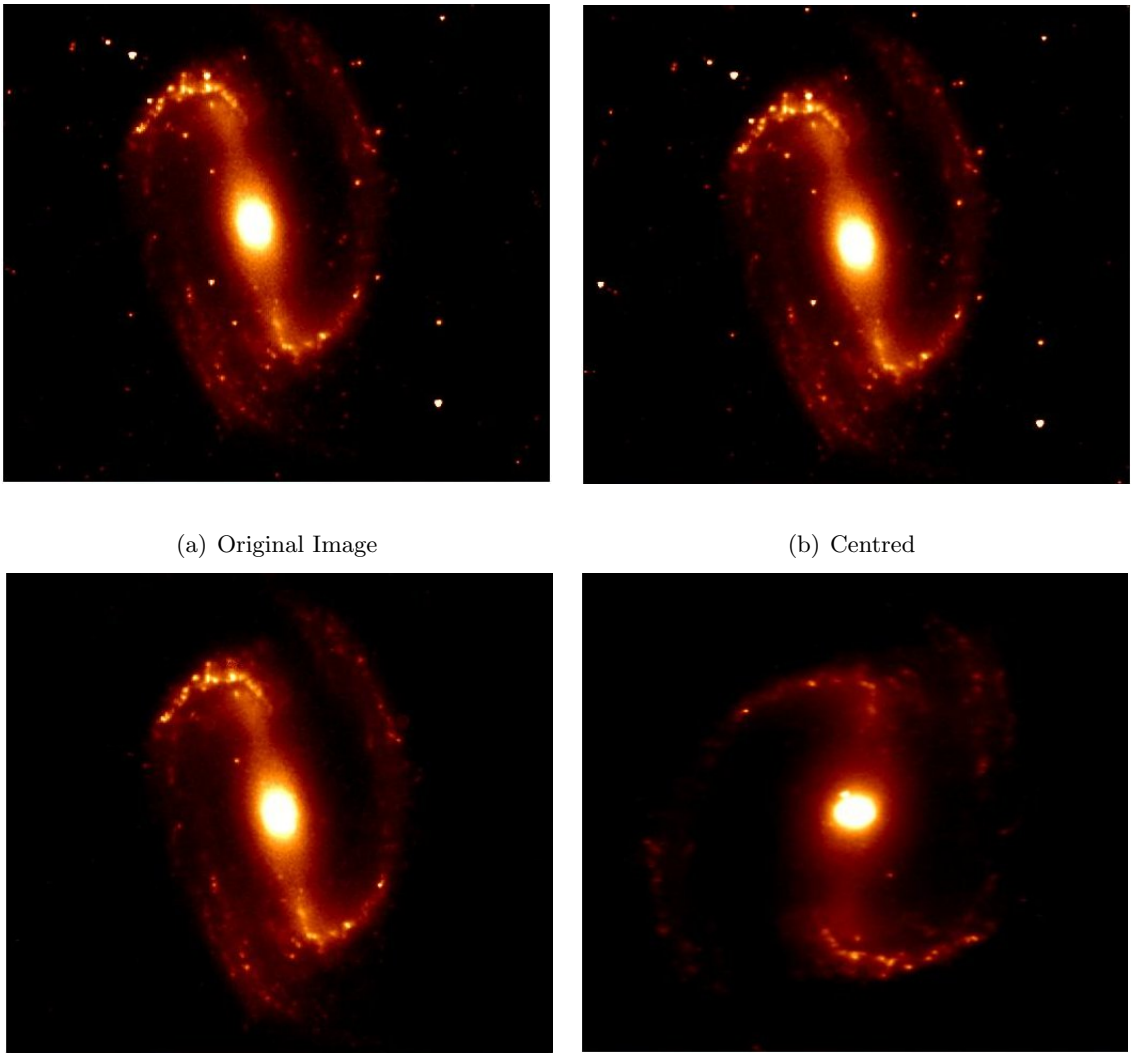

(a) Original Image (b) Centred

(c) Star Cleaned (d) Deprojected

Figure 3.1: Preparation for Deprojection of NGC1300

A side effect of deprojection is that often the galaxy's bulge becomes artificially stretched. An important concern in the application of the GTM is how to prevent this artificial bulge stretch from affecting the derived Q_g. As a first approach, the bulge can be approximated with a seeing-convolved spherical density distribution, separated from the galaxy image before the disk deprojection and the calculation of disk forces. For this purpose a three-component 2D decomposition can be used, including a Ferrers bar besides an exponential disk and a Sersic bulge. Although the bar model is rather crude, its inclusion to the fit is often crucial to prevent bar light from being assigned into unrealistically large bulges (see Peng et al. 2002, who also stress the insufficiency

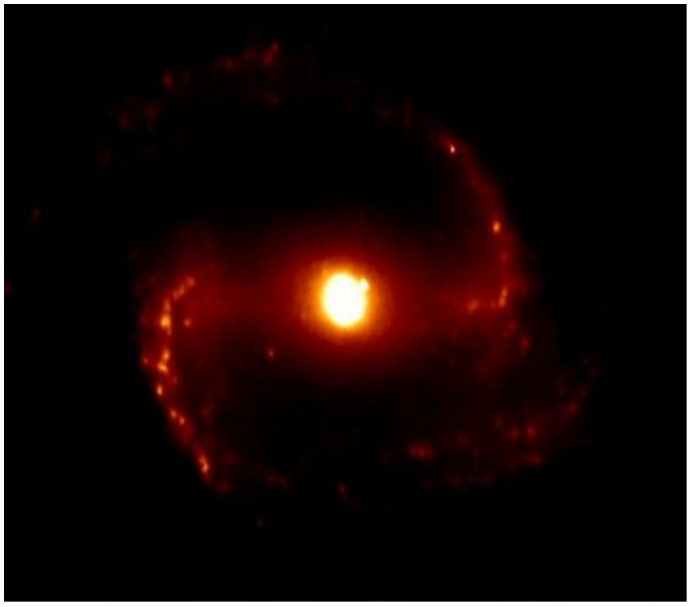

Figure 3.2: Centered, star-cleaned, deprojected, $2^n \times 2^n$ dimensional image of NGC1300 as required for Potential calculation by Quillen, Frogel & González (1994).

of 2-component models). However, comparison to force evaluations without any special treatment of bulges shows that the overall effect of bulge stretch is small (Laurikainen et al. 2004, Buta et al. 2004), as has been assumed in this dissertation.

3.6 Results & Discussion

One of the most dramatic, new results, of this dissertation is shown in Figure 3.3, compiled with a sample of 40 galaxies. The distribution of maximum relative gravitational torques is plotted for galaxy images at 3.6μm against 4.5μm. The number frequency of the resulting Q_g values, for both 3.6 μm and 4.5 μm is shown in Figure 3.4 for the full sample. Both the plot and corresponding histogram show that there is a very strong correlation between maximum torques across a full spread in Q_g for the 3.6μm - 4.5μm spectral window. The positions of the force maxima for each galaxy pair in our sample are exhaustively detailed in Figure 3.5. Regardless of the strength of a bar, galaxies imaged at 3.6μm have very similar, if not near-identical values for Q_g from those imaged at 4.5μm. Image pairs (i.e.: images of the same galaxy compared at both 3.6μm and 4.5μm) therefore have an underlying stellar backbone morphology which is stable and constant over at least the 0.9μm difference between both passbands mentioned. Figure 3.4 shows the spread in Q_g values, from 0.03 in the case of NGC3368

to 0.72 for NGC7741, over which this correlation holds. The maximum relative gravitational torques are listed in Table 3.3 for individual galaxies. From the histogram in Figure 3.4, it is clear that the sample itself is biased toward strongly barred galaxies, as compared with, for example, results from Buta et al. (2004) who find a primary peak in a similar plot for their sample, an asymmetry these authors claim to be due mainly to the prevalence of SA and SAB galaxies. They also note the existence of an "extended tail" due to SB galaxies. A comparison between the histograms derived by Block et al. (2002), Buta et al. (2004) and this dissertation is highly appropriate because they all use the same procedure to determine Q_g values by making use of the potential code by QFG. Statistically, the sample sizes of Block et al. (2002), namely 163, and Buta et al. (2004), 180, are approximately four times as large as the 40 used here. The main reason for this limitation is the lack of available images with suitable orientation parameters (such as an inclination cut-off of 70 degrees).

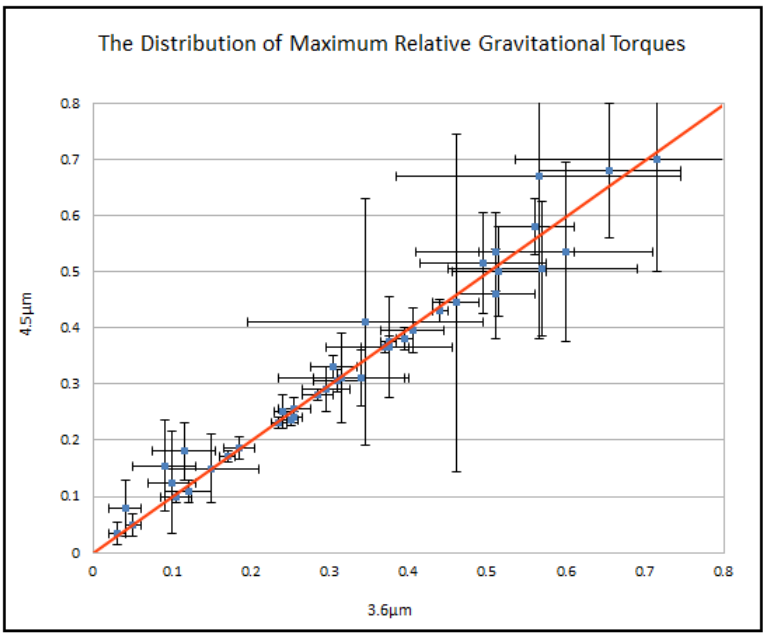

Figure 3.3: The distribution of maximum relative gravitational torques of image pairs between $3.6\mu m$ and $4.5\mu m$. There is a tight coupling of morphology in all galaxy pairs in our sample across a wide range of Q_g values.

The main differences in the histograms is attributed to the artificial selection biases imposed on the respective samples. Buta et al. (2004) show more galaxies having a low maximum relative torque ($Q_g \approx 0.15$) whereas the first two bins in the Block et al. (2002) histogram are extremely deficient. Buta et al. (2004) proposed the reason for the observed deficiency to be their lack of a bulge/disk composition, whereby deprojection

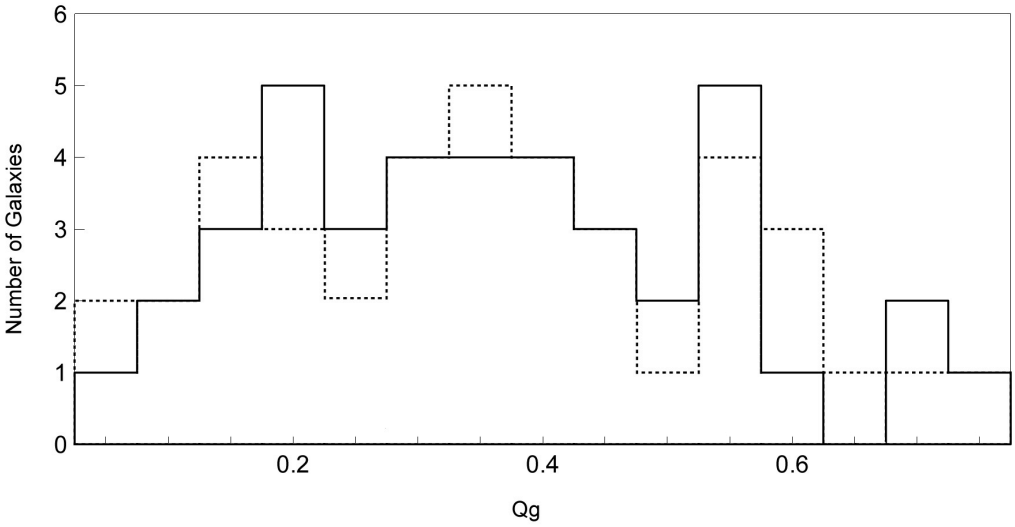

Figure 3.4: Observed number frequency of $3.6\mu m$ (solid line) and $4.5\mu m$ (dotted line) gravitational torques in our sample.

stretch can depopulate the first two bins. However, the effect seems less important than might have been expected given that our inclination cutoffs were high in both cases, and a significant fraction of galaxies in Table 3.3 show a moderate or low Q_g, even though the inclination cut-off used was also 70 degrees. While Buta et al. (2004) argue that a more serious effect on the relative frequency of observed Q_g values could be due to the assumed scale heights, for the purposes of comparing 3.6μm morphology with that of 4.5μm, such considerations are far less important than ensuring that identical analysis parameters were used. It is well understood that a decrease in scale height, leads to an increase in Q_g. The "max h_z" case clearly shows a systematic reduction in Q_g values when compared with the "min h_z" case (Block et al., 2002). However, worst case scenarios suggest that the effect typically only changes the Q_g values by one torque "class". These authors used $h_R/h_z = 12$ for all galaxies irrespective of Hubble type, and their analysis favored lower vertical scale heights and larger values of Q_g on average, whereas Buta et al. (2004) used bulge/disk decompositions and a type dependence to h_R/h_z resulting, on average, in vertical scale heights being higher. This had the systematic effect of producing weaker gravitational torques. For a more objective comparison, Buta et al. (2004) computed Q_g by assuming $h_z = h_R/12$, which resulted in a partial depletion of the first two bins. The comparison, however, did not account for all the differences seen in Block et al. (2002).

Table 3.3: Maximum Relative Gravitational Torque

Galaxy	**Type(RC3)**	Q_{T_1}	**Error**	Q_{T_2}	**Error**
NGC0289	SB(rs)bc	0.15	0.06	0.15	0.06
NGC0600	(R')SB(rs)d	0.34	0.06	0.31	0.05
NGC0613	SB(rs)bc	0.52	0.06	0.5	0.08
NGC0685	SAB(r)c	0.35	0.15	0.41	0.22
NGC0936	$SB0^+$(rs)	0.25	0.01	0.24	0.01
NGC0986	SB(rs)ab	0.51	0.1	0.54	0.07
NGC1300	SB(rs)bc	0.57	0.12	0.51	0.12
NGC1326	(R)$SB0^+$(r)	0.17	0.01	0.17	0.01
NGC1365	SB(s)b	0.05	0.01	0.05	0.02
NGC1398	(R')SB(r)ab	0.26	0.02	0.26	0.02
NGC1433	(R')SB(r)ab	0.38	0.01	0.38	0.01
NGC1493	SB(r)cd	0.32	0.08	0.31	0.08
MGC1512	SB(r)a	0.24	0.01	0.23	0.01
NGC3198	SB(rs)c	0.19	0.02	0.19	0.02
NGC3319	SB(rs)cd	0.56	0.05	0.58	0.05
NGC3368	SAB(rs)ab	0.03	0.01	0.04	0.02
NGC3504	(R)SAB(s)ab	0.51	0.05	0.46	0.08
NGC3513	SB(rs)c	0.38	0.08	0.37	0.09
NGC3627	SAB(s)b	0.09	0.04	0.16	0.08
NGC3892	$SB0^+$(rs)	0.12	0.03	0.11	0.02
NGC4245	SB(r)0/a:	0.11	0.02	0.1	0.01
NGC4394	(R)SB(r)b	0.26	0.01	0.24	0.01
NGC4421	SB(s)0/a	0.3	0.03	0.29	0.04
NGC4450	SA(s)ab	0.12	0.04	0.18	0.05
NGC4535	SAB(s)c	0.46	0.03	0.45	0.3
NGC4548	SB(rs)b	0.42	0.02	0.43	0.02
NGC4593	(R)SB(rs)b	0.04	0.02	0.08	0.05
NGC4596	$SB0^+$(r)	0.4	0.01	0.37	0.09
NGC5101	(R)SB(rs)0/a	0.44	0.01	0.43	0.02
NGC5371	SAB(rs)bc	0.31	0.03	0.33	0.02
NGC5375	SB(r)ab	0.31	0.03	0.31	0.02

Continued on next page

Table 3.3 – continued from previous page

Galaxy	Type(RC3)	Q_{T_1}	Error	Q_{T_2}	Error
NGC5383	(R')SB(rs)b:pec	0.66	0.09	0.68	0.12
NGC5921	SB(r)bc	0.5	0.08	0.52	0.09
NGC6217	(R)SB(rs)bc	0.57	0.18	0.67	0.29
NGC6744	SAB(r)bc	0.24	0.01	0.25	0.03
NGC7329	SB(r)b	0.37	0.03	0.37	0.01
NGC7479	SB(s)c	0.1	0.03	0.13	0.09
NGC7552	(R')SB(s)ab	0.6	0.11	0.54	0.16
NGC7741	SB(S)cd	0.72	0.18	0.7	0.2
IC1438	(R')SAB(rs)a	0.29	0.02	0.28	0.01

The average value of Q_g for all 40 galaxies used in this dissertation is 0.33 with a standard deviation of 0.18. Buta et al. (2004) find an average of Q_g of 0.222 for their full sample, with a standard deviation of 0.147. This compares well with the distribution of maximum relative gravitational torques found in the Ohio State University Bright Galaxy Survey (OSUBGS) sample (Block et al. 2002). The inclination cut-off as used by Block et al. (2002) was 70 degrees as inferred from the RC3 $logR_{25}$ values, whereas Buta et al. (2004) made use of isophotal fits to accept galaxies with inclinations less than 65 degrees. In this dissertation vertical exponential scale height profiles were assumed, and a scale height of 325pc was chosen as a first approximation. This assumption is sensible, as images at both 3.6μm and 4.5μm were analyzed using identical scale, distance and inclination data. Furthermore, no bulge/disk decompositions were made as this would have masked any morphological discrepancies that may occur in the bulge region between the two bands. Most of the orientation parameters used for deprojection were obtained from the RC3 (de Vaucouleurs et al. 1991).

A number of technical issues should be brought to reader's attention:

- The number of Fourier terms beyond $m = 20$ has little impact, as most of the smoothing is already evident when only the first 6 terms are used.
- Buta & Block (2001) show the impact of the position angle of the bar relative to the line of nodes, such as for the case of NGC 1300, where the bar is oriented nearly

along the line of nodes. Here the maximum torque is sensitive to inclination. While such a rigorous analysis has not been performed for the sample used in this dissertation, Buta et al. (2004) find that there is indeed a bias detected where the average bar strength is weaker for those systems where the bar becomes progressively more stretched along the minor axis during deprojection.

- The question as to whether a Cartesian approach (as used in this dissertation), versus the polar method used by Buta et al. (2004), could result in significant differences in the computed Q_g values is considered here. Comparison of Buta et al. (2004) with Block et al. (2002) show that some Cartesian Q_g values are noticeably larger than the polar grid values. However, as discussed in Laurikainen & Salo (2002), the Cartesian method can lead to large spurious force values in the noisy outer parts of images, sometimes leading to an overestimate of Q_g. These spurious force values have not been encountered with the analysis presented here, partially due to small refinements made to the GTM code, particularly making it more suitable for lower resolution images, and also due to the care taken to include a large region of cleaned "sky" surrounding the galaxies. A more quantitative audit on the difference between the Cartesian method and the polar counterpart is presented in Buta et al. (2004). Here these authors compare Q_g values of three highly inclined galaxies, NGC3166, NGC3338 and NGC3675, calculated using the polar method, to that obtained by Block et al. (2002) using the Cartesian method. This comparison revealed a strong correlation between the two methods.

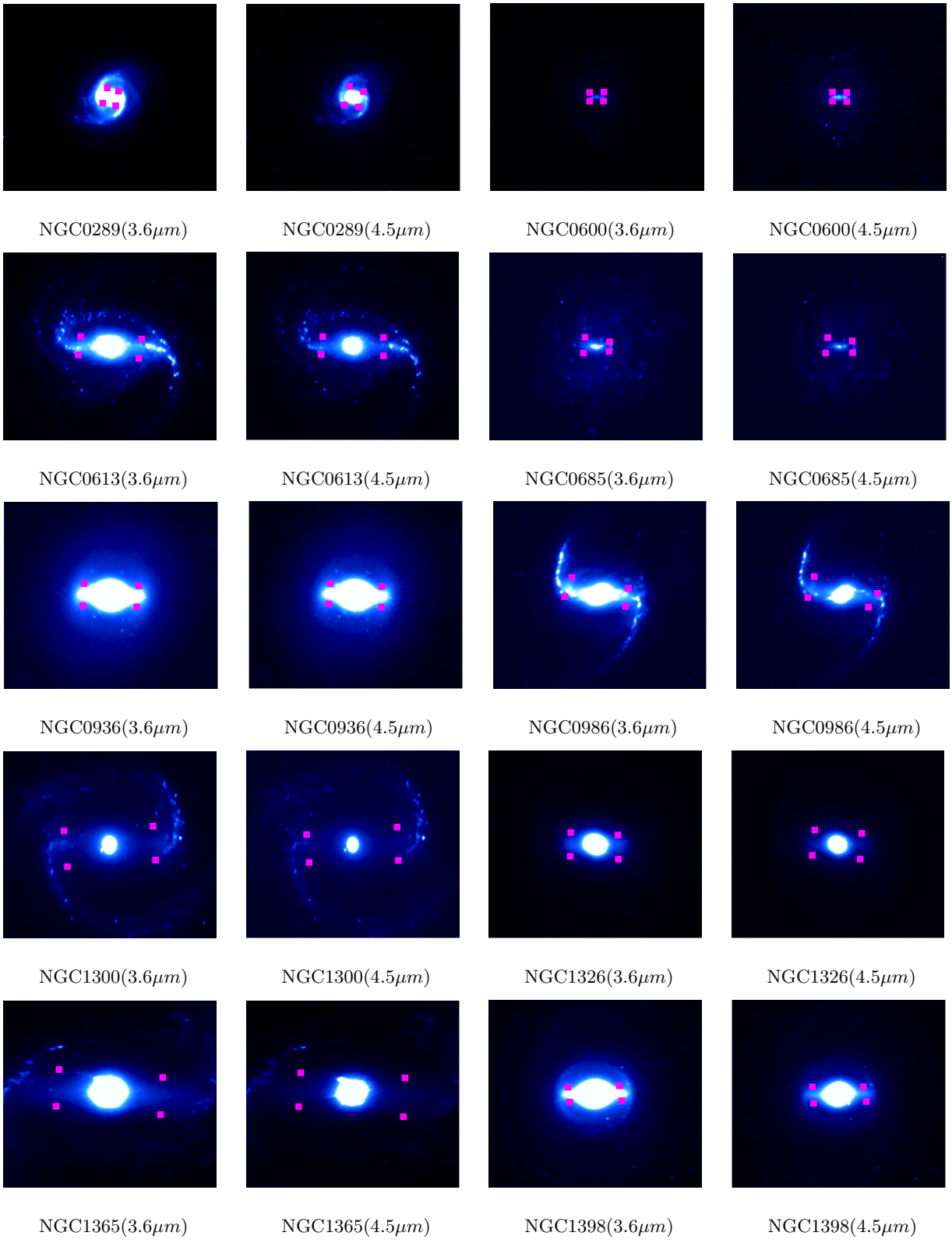

Figure 3.5: Torque maxima positions for 3.6μm and 4.5μm image pairs.

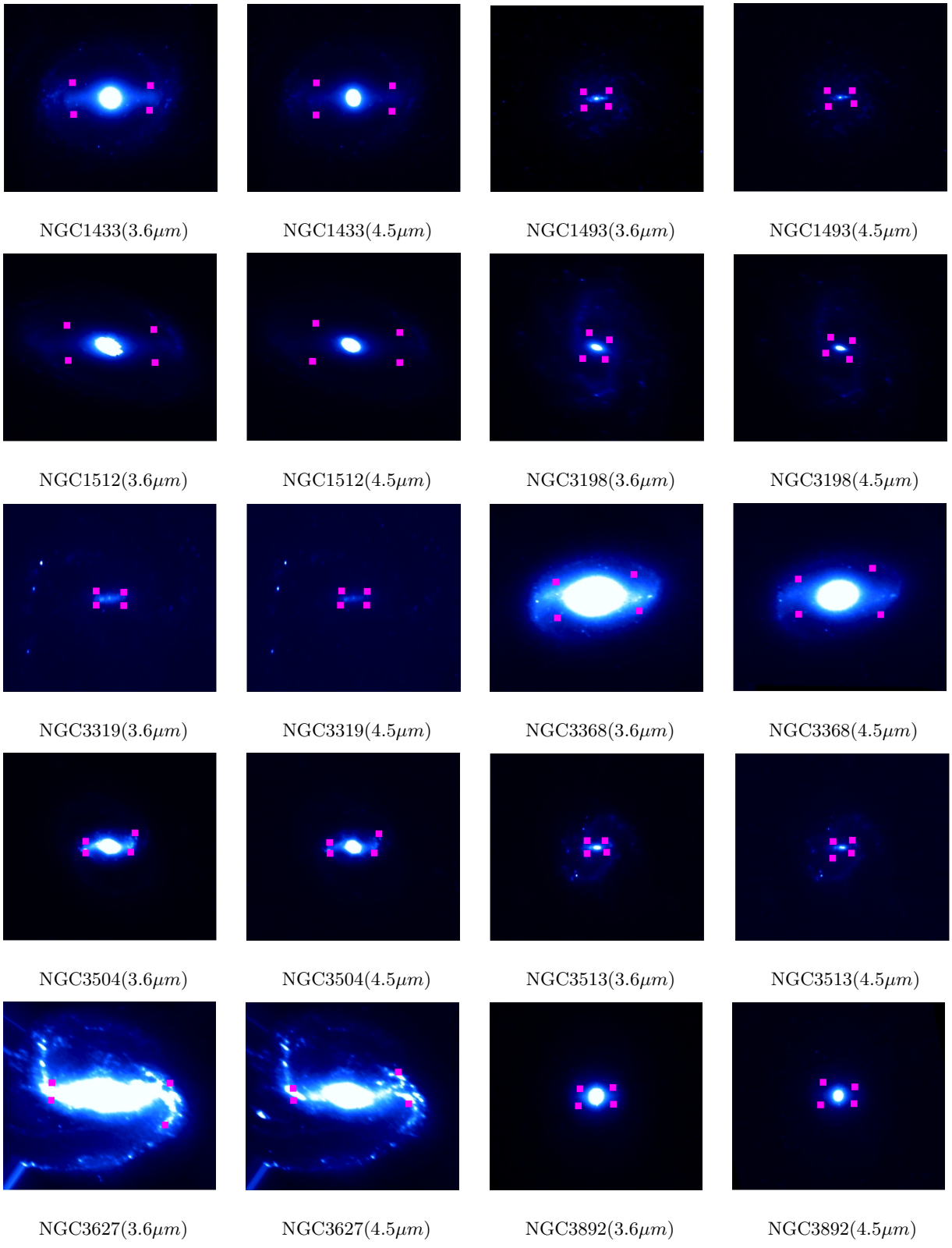

NGC1433(3.6μm) NGC1433(4.5μm) NGC1493(3.6μm) NGC1493(4.5μm)

NGC1512(3.6μm) NGC1512(4.5μm) NGC3198(3.6μm) NGC3198(4.5μm)

NGC3319(3.6μm) NGC3319(4.5μm) NGC3368(3.6μm) NGC3368(4.5μm)

NGC3504(3.6μm) NGC3504(4.5μm) NGC3513(3.6μm) NGC3513(4.5μm)

NGC3627(3.6μm) NGC3627(4.5μm) NGC3892(3.6μm) NGC3892(4.5μm)

Figure 3.5: Torque maxima positions for 3.6μm and 4.5μm image pairs (Continued).

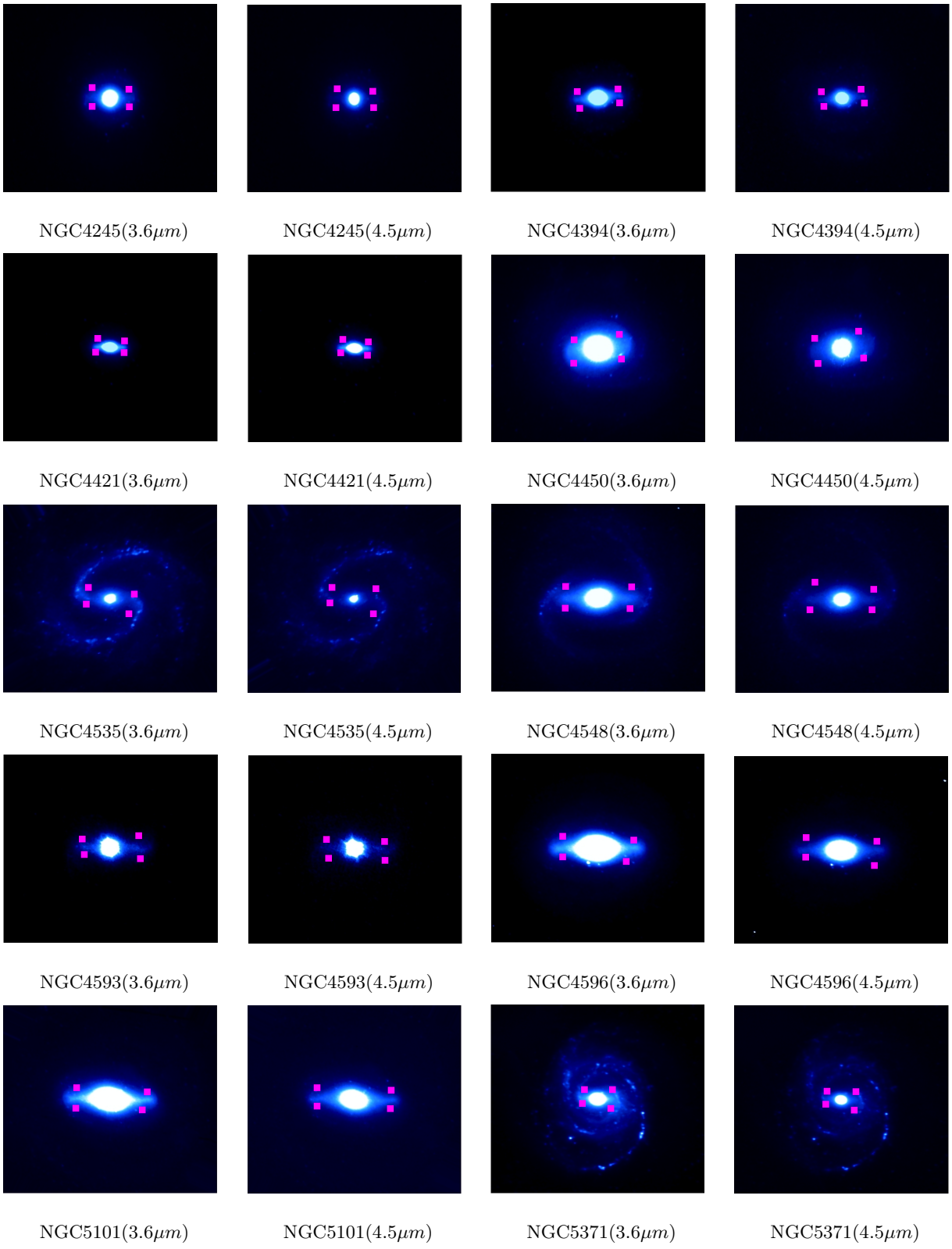

NGC4245(3.6μm) NGC4245(4.5μm) NGC4394(3.6μm) NGC4394(4.5μm)

NGC4421(3.6μm) NGC4421(4.5μm) NGC4450(3.6μm) NGC4450(4.5μm)

NGC4535(3.6μm) NGC4535(4.5μm) NGC4548(3.6μm) NGC4548(4.5μm)

NGC4593(3.6μm) NGC4593(4.5μm) NGC4596(3.6μm) NGC4596(4.5μm)

NGC5101(3.6μm) NGC5101(4.5μm) NGC5371(3.6μm) NGC5371(4.5μm)

Figure 3.5: Torque maxima positions for 3.6μm and 4.5μm image pairs (Continued).

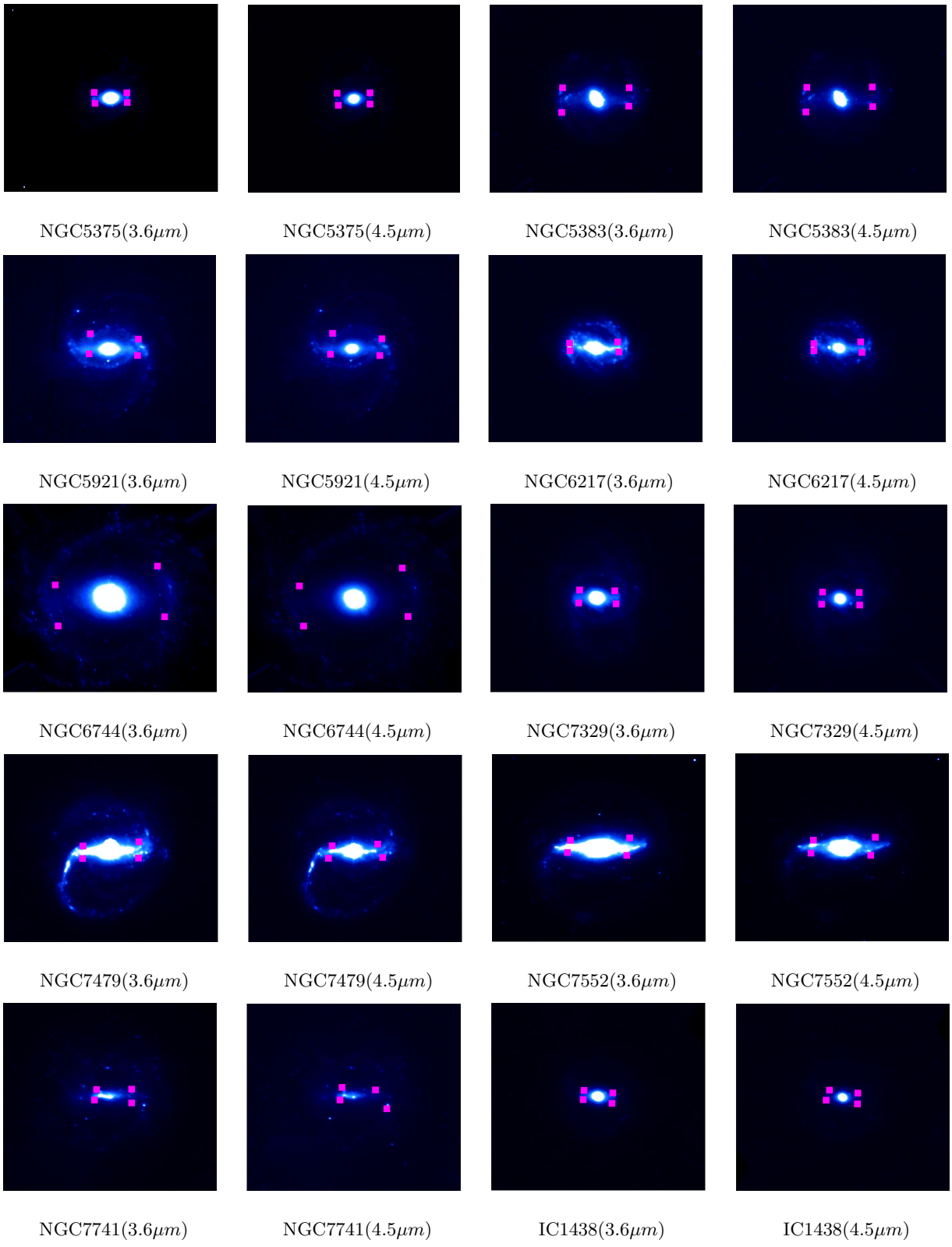

Figure 3.5: Torque maxima positions for 3.6μm and 4.5μm image pairs (Continued).

Chapter 4

Isophotal Ellipses

"The truth may be puzzling. It may take some work to grapple with. It may be counterintuitive. It may contradict deeply held prejudices. It may not be consonant with what we desperately want to be true. But our preferences do not determine what's true"

-Carl Edward Sagan

"Joy in looking and comprehending is nature's most beautiful gift."

-Albert Einstein

4.1 Galactic Isophotes

Galactic isophotes are contour lines of average surface brightness of a galaxy. It is assumed that a given isophote can be approximated by an ellipse (Kent 1983), which can be fitted to all the data points to extract the intensity level from the galaxy. Galactic isophotes are overlaid on a galaxy image using the IRAF routine ELLIPSE which returns ellipticity, surface brightness and position angle profiles. These profiles are then used to identify bars and characterize their sizes and ellipticities. It also gives reliable structural parameters on conditions that can be interpreted in terms of these various profiles.

The technique of ellipse fitting is widely used to study the morphology of underlying structures of elliptical and barred spiral galaxies at optical as well as at NIR wavelengths. It was initially implemented on elliptical galaxies (Kent 1983), and was later implemented on a set of 10 early type *barred* spiral galaxies at optical wavelengths to study morphological properties of bars (Wozniak et al. 1991). Zheng et al. (2005) detected the bar structure for their sample of HST images in order to investigate the

effects of bar-driven secular process in the evolution of galaxy morphology. Barazza et al. (2007) characterized bars using R-band images from Sloan Digitized Sky Survey.

Isophotal ellipse fitting is well suited to detecting the presence of bars in NIR images to avoid bar classification problems such as subjectivity, low resolution, and contamination by dust. For instance, Regan & Elemegreen (1997) investigate bar and arm structures of barred spiral galaxies imaged at K-band and Knapen et al. (2000) determine the presence of bars in a CFA sample of Seyfert galaxies to investigate the correlation between the presence of bars and the presence of nuclear activities at the centre of galaxies. Laine et al. (2002) use ellipse fitting to identify bars in HST H-band images to classify galaxies using various profiles traced by isophotes of galaxies. Marinova & Jogee (2007) characterize the frequency and structural properties of bars in the local universe at optical and NIR wavelengths by fitting ellipses to $B-$ & $H-$band images of the Ohio State University Bright Spiral Galaxy Survey of 180 spirals. In here they present results on the bar fraction at $z \sim 0$, its dependence on Hubble type, the distribution of bar sizes and strengths as characterized by ellipse-fitting and variation of bar properties along the Hubble sequence.

Fractions of bars in nearby barred spiral galaxies were also measured by Menéndez-Delmestre et al. (2007) using J, H, and K_s band images of 151 spiral galaxies from theTwo Micron All Sky Survey (2MASS). They used this sample to study the evolution of bar fractions and bar properties with increasing redshift. These authors detected bars by analyzing the full two-dimensional light distribution and combined signature of ellipticity and position angle, where the presence of bars was detected using ellipticity and position angle profiles. They found that within the bar region the position angle remains constant as the ellipticity increases monotonically. In their sample of 151 galaxies they found that 89 displayed ellipticity and position angle signatures characteristic of barred spirals, i.e. 59%.

In this dissertation we identify a correlation between the gravitational torque method and the ellipse fitting method for 28 S^4G (Spitzer Survey of Stellar Structures in Galaxies) images observed at $3.6\mu m$. This sample of galaxies was used to perform an isophotal ellipse fitting analysis and the results obtained were compared with the results of Q_g . This comparison has shed insight into the relationship between the gravitational torques and the luminous contribution of bars at near-infrared and has provided a way to estimate bar strengths for more distant galaxies at rest frame $3.6\mu m$, where the data is more noisy.

4.2 Properties of S^{4}G galaxies

The Spitzer Survey of Stellar Structures in Galaxies (S^{4}G) consist of 2331 nearby galaxies, observed at $3.6\mu m$ and $4.5\mu m$ using the Infrared Array Camera (IRAC). These galaxies are $d < 40Mpc$ ($z <\sim 0.01$, for $H_0 = 75kms^{-1}Mpc^{-1}$). The exposure time for each galaxy was $240s$ and were then mapped to $\geq 1.5 \times D_{25}$. The 1σ noise level at $3.6\mu m$ and $4.5\mu m$ is 0.0072 and $0.0093MJysr^{-1}$ respectively. The sample has a mean stellar mass surface density of $\sim 1M_{\odot}pc^{-2}$, which makes it ideal for the study of mass distribution as well as stellar structures in galaxies.

Of these 2331 galaxies we have selected 21 nearby barred spiral galaxies with inclination $< 65^{\circ}$ (according to the Third Reference Catalogue of Bright Galaxies (RC3)), imaged at $3.6\mu m$. The sample also includes 7 nearby barred spirals with inclination $< 70^{\circ}$ from the Spitzer IRAC archive, also imaged at $3.6\mu m$. It contains 23 SB and 5 SAB galaxies as described in de Vaucouleurs et al. (1991). In the sample, 12 galaxies have a plate scale of $1.22arcsec/pix$, 11 have a plate scale of $0.6arcsec/pix$ and 5 have a plate scale of $0.75arcsec/pix$. These parameters as well as the distances to these galaxies can be found in Table 4.1. The original images have different sizes but were all reduced to size 512×512 as described in the previous chapter.

Table 4.1: Properties of the S^4G sample (T&F = Tully & Fisher 1987 ; T= Tully 1988)

Galaxy	**Type (RC3)**	**Incl. (degrees)**	**dist. (Mpc)**	**dist.ref**	**plate scale(arcsec/pix)**
NGC0600	(R')SB(rs)d	31.66	22.9	T&F	0.75
NGC0685	SAB(r)c	26.97	15.2	T	1.22
NGC0936	$SB0^+$(rs)	29.43	16.9	T	1.22
NGC0986	SB(rs)ab	40.66	23.2	T&F	1.22
NGC1187	SB(r)c	42.16	16.3	T&F	1.22
NGC1300	SB(rs)bc	48.65	18.8	T&F	1.22
NGC1326	(R)$SB0^+$(r)	42.16	16.9	T&F	1.22
NGC1398	(R')SB(r)ab	40.66	16.1	T&F	1.22
NGC1433	(R')SB(r)ab	24.21	11.6	T&F	1.22
NGC3351	SB(r)b	47.46	8.1	T&F	1.22
NGC3892	$SB0^+$(rs)	40.66	27.2	T	0.75
NGC4245	SB(r)0/a:	40.66	9.7	T	1.22
NGC4548	SB(rs)b	37.41	16.8	T&F	1.22
NGC4596	$SB0^+$(r)	42.16	16.8	T&F	0.75
NGC5375	SB(r)ab	31.66	37.8	T&F	0.75
NGC5921	SB(r)bc	35.63	25.2	T&F	0.75
NGC7552	(R')SB(s)ab	37.41	19.5	T&F	1.22
NGC0289	SB(rs)bc	44.93	19.4	T&F	0.6
NGC4535	SAB(s)c	44.93	16.8	T&F	0.6
NGC6217	(R)SB(rs)bc	33.72	23.9	T&F	0.6
NGC6744	SAB(r)bc	49.79	10.4	T&F	0.6
IC1438	(R')SAB(rs)a:	31.66	33.8	T&F	0.6
NGC613	SB(rs)bc	40.66	17.5	T&F	0.6
NGC3198	SB(rs)c	67.10	10.8	T&F	0.6
NGC4421	SB(s)0/a	40.66	16.8	T&F	0.6
NGC5101	(R)SB(rs)0/a	31.66	27.4	T&F	0.6
NGC5371	SAB(rs)bc	37.41	37.8	T&F	0.6
NGC7329	SB(r)b	47.46	42.1	T&F	0.6

4.3 Ellipse Fitting Method

Kent (1983) used a similar ellipse fitting technique to that of Young et. al (1979) and presented various profiles as functions of radius along the major axis of M31. He described intensity of the galaxy everywhere as

$$I = I(s) \tag{4.1}$$

where the radius s is

$$s^2 = \tilde{x}^2 + \frac{\tilde{y}^2}{(1-\epsilon^2)} \tag{4.2}$$

and

$$\tilde{x} = (x - x_c)\cos\theta + (y - y_c)\sin\theta \tag{4.3}$$

$$\tilde{y} = (y - y_c)\cos\theta + (x - x_c)\sin\theta \tag{4.4}$$

where (x_c, y_c) is the centre of the ellipse, θ is the position angle of the major axis and ϵ is the ellipticity ($\epsilon = 1 - b/a$), where a and b are semi-major and semi-minor axis lengths respectively. For a given semi-major axis length, initial guesses are made for x_c, y_c, θ, and ϵ and the intensity in the galaxy image around this ellipse is sampled at equal intervals in the eccentric anomaly E.

$$x = a_0 \cos E \tag{4.5}$$

$$y = a_0(1 - \epsilon_0)\sin E \tag{4.6}$$

Then the intensity along this trial ellipse is measured by using weighted least-squares fitting technique.

$$I = I_0 + A_1 sin(E) + B_1 cos(E) + A_2 sin(2E) + B_2 cos(2E) \tag{4.7}$$

The corrections to the four ellipse parameters are dependent on the Fourier coefficients A_1, B_1, A_2, and B_2 and can be found in Kent (1983).

4.4 Step by Step Procedure

- For each image centre the galaxy image
- Remove foreground stars
- Deproject the image
- Determine galaxy centre
- Fit ellipses
- Use generated radial profiles of surface brightness, ellipticity, and position angle to classify galaxies as barred or unbarred and measure the bar strength and size

$3.6\mu m$ Spitzer IRAC images were analyzed using the above mentioned procedure. All the images in the sample were cleaned of foreground stars by average background replacement using a circular aperture. The images were centered and deprojected as described in Appendix A. This was done to ensure that the input images for the GTM analysis and ellipse fitting analysis would be the same. The centers of galaxies were determined using the the IRAF routine IMEXAM and the IRAF task ELLIPSE (Jedrzejewski, 1987) was used to fit ellipses to each image with a radial increment of 2 arcsecs. The radial profiles that were generated by the ellipse fitting task were then used to classify galaxies as barred or unbarred. In order to classify galaxies as barred the following criteria must be satisfied:

ϵ increases steadily to a global maximum, while the P.A values remain constant and at the transition from the bar to disk region ellipticity drops by at least 0.1 with changes in P.A (see Figure 4.2).

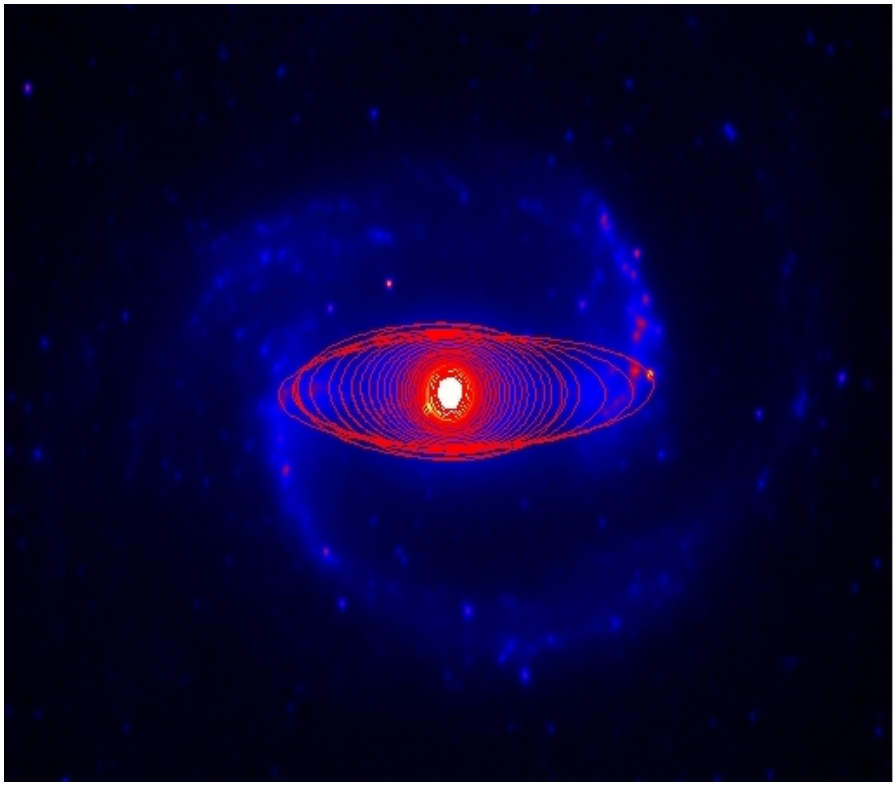

Figure 4.1: Isophotal ellipse contours for increments in radius superimposed over a $3.6\mu m$ deprojected image of NGC1300. Ellipse contours have the highest ellipticity over the bar region, the maximum of which is used to define ϵ_{max}.

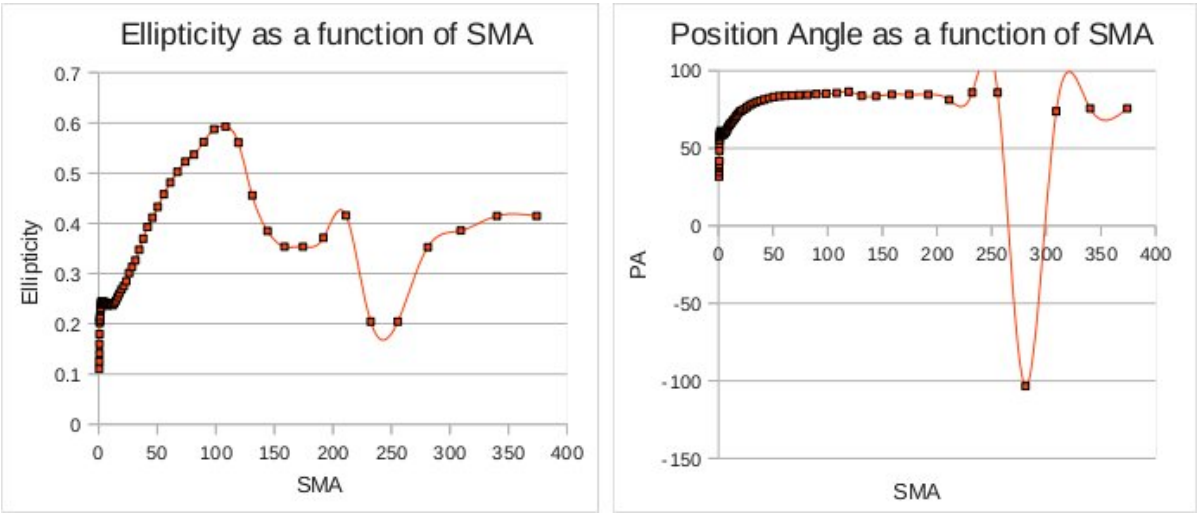

Figure 4.2: Ellipticity and Position angle profiles of NGC5101 reveal the signature of a bar as defined by the following criteria: Ellipticity increases monotonically as a function of the semi-major axis radius until reaching a maximum (ϵ_{max}) - the bar strength. The position angle remains fairly constant within this bar region. NGC 5101 has a bar strength of 0.6.

The maximum ellipticity, ϵ_{max}, used as a measure of bar strength can be used to group galaxies into two different bins, strongly barred and weakly barred (e.g. Athanassoula, 1992; Martin, 1995; Wozniak et al. 2000; Jogee et al. 1999, 2002a&b; Knapen et al. 2000; Laine et al. 2002). Strong bars are defined in the interval $0.50 \leq \epsilon_{max} \leq 0.75$ and weak bars in the interval $0.25 \leq \epsilon_{max} \leq 0.40$ (Marinova & Jogee, 2007). The application of this method is suitable for local galaxies as well as galaxies out to intermediate redshifts (Jogee et al. 2004; Elmegreen et al. 2004).

4.5 Results & Discussion

The maximum deprojected ellipticity is a simple and accessible measure of bar strength, and hence the isophotal ellipse fitting method used in this dissertation is robust in detecting a bar signature for all galaxies in our sample. The higher the measured isophotal ellipticity of the bar, the greater the effect the bar potential has on the mean axisymmetric gravitational potential of the disk. Like Laurikainen et al. (2002) and Block et al. (2004) we found a strong correlation between the ϵ_{max} and the Q_g parameter, which in essence is a measure characterizing the maximum gravitational bar torque relative to the background galactic disk (Buta & Block 2001). The mean bar isophotal ellipticity in our sample is 0.59 with a standard deviation of 0.10. The distribution of ellipticities clearly favors higher values - the result of a bias toward strongly barred galaxies in our sample. There is a noticeable absence of bars with "low" ellipticity, correlating well with the definition of a bar as described in Menéndez-Delmestre et al. (2007). Strong bars, i.e.: those with a high ellipticity, are the easiest to identify. We suspect the sharp decline beyond $\epsilon \sim 0.7$, is an intrinsic geometric property of the bar, and not an indication of a lack of strong bars in our sample. Menéndez-Delmestre et al. (2007) find a weak correlation between bar size and bar strength in terms of the bar semimajor axis ratio a_{bar}/R_{25}. These authors find that stronger bars also appear to be the longest ones in absolute size and relative to the size of the disk in which they are embedded. A trend they find to be more significant for early-type barred galaxies compared to late types. While there are cases where the method may fail to detect a bar - particularly in the case of small bars - these authors argue this is unlikely to be statistically significant in the case of the majority of galaxies classified using this method.

As the sample in this dissertation is biased toward nearby bright barred galaxies,

all galaxies display a bar signature as defined by Menéndez-Delmestre et al. (2007). They define the relative bar size, a_{bar}/R_{25}, to be the ratio of the bar semimajor axis compared with the RC3 radius of the host galaxy at a B magnitude of 25 (R_{25}). An advantage of using a relative bar size is that of being a distance-independent measure. The error on the relative bar size is dominated by the uncertainty on the measurement of the bar signature from the ellipticity profile, at approximately the 10% level. These authors find that 90% of all bars within the sample extend out to less than 50% of the galaxy disk radius. They find a trend of relative bar sizes, with early-type bars being significantly larger than late types. Bars in early type spirals have a median a_{bar}/R_{25} a factor of 2 larger than bars in late types.

However Laurikainen et al. (2002) suggest that ellipticity is not a full description of bar strength since the value of ϵ_{max} is independent of the mass of a galaxy/bar. Instead these authors recommend that the gravitational torque method may be better to evaluate the measure of bar strength as it is influenced by the mass and shape of the bar when determining the magnitudes of the gravitational torques at each point. The other disadvantage of the ellipse fitting algorithm is that it relies on a smooth light intensity distribution and often fails for an irregular distribution (Menéndez-Delmestre et al. 2007).

There are several advantages and disadvantages when it comes to using the aforementioned schemes. The disadvantage of using the Q_g method is that it is dependent on the mass-to-light ratio assumption, the scale height of the disk, as well as the ability to derive reliable potentials using images, which raises difficulty in applying the method to a large number of intermediate-redshift galaxies due to resolution and signal to noise ratio issues. Whereas the ellipse fitting method estimates bar strength without making any assumption about the mass-to-light ratio of the galaxy or its scale height, which of course means that the bar strength of intermediate redshift galaxies can be estimated.

For this dissertation, the maximum gravitational torque (Q_g) and the maximum ellipticity (ϵ_{max}) values are used as a measure of bar strength to find a correlation between the two methods, results of which are displayed in Table 4.2. We find an increase in Q_g values with a decrease in axis ratio (b/a) (see Figure 4.4), and compare our results with that of Block et. al (2001), Laurikainen et al. (2002) and Buta et al. (2004). We find our results correlate well with Laurikainen et al. (2002) and have less scatter than that of Block et al. (2001). The scattering in Block et al. (2001) has been attributed to the high uncertainty in the (b/a) values, based on blue photographic

plates, that these authors used. The relation we find between Q_g and ϵ_{max} reveals an underlying correlation between the non-axisymmetric gravitational field and the overall morphology of the bar. We find that strong bars i.e.: those with high values for Q_g, have lower isophotal bar-axis ratios (b/a).

Table 4.2: Bar Strengths described by Q_g and ϵ_{max}

Galaxy	**Type (RC3)**	Q_g	**error**	ϵ_{max}	**error**	$b/a = 1 - \epsilon_{max}$
NGC0600	(R')SB(rs)d	0.28	0.1	0.67	0.01	0.33
NGC0685	SAB(r)c	0.32	0.12	0.69	0.02	0.31
NGC0936	$SB0^+$(rs)	0.27	0.02	0.5	0.0	0.5
NGC0986	SB(rs)ab	0.5	0.1	0.69	0.01	0.31
NGC1187	SB(r)c	0.26	0.08	0.61	0.01	0.39
NGC1300	SB(rs)bc	0.66	0.16	0.71	0.01	0.29
NGC1326	(R)$SB0^+$(r)	0.18	0.02	0.48	0.01	0.52
NGC1398	(R')SB(r)ab	0.28	0.02	0.51	0.01	0.49
NGC1433	(R')SB(r)ab	0.34	0.01	0.62	0.0	0.38
NGC3351	SB(r)b	0.3	0.01	0.62	0.01	0.38
NGC3892	$SB0^+$(rs)	0.11	0.05	0.31	0.0	0.69
NGC4245	SB(r)0/a:	0.12	0.05	0.39	0.01	0.61
NGC4548	SB(rs)b	0.44	0.05	0.62	0.0	0.38
NGC4596	$SB0^+$(r)	0.4	0.01	0.6	0.0	0.4
NGC5375	SB(r)ab	0.3	0.06	0.51	0.01	0.49
NGC5921	SB(r)bc	0.37	0.04	0.72	0.01	0.28
NGC7552	(R')SB(s)ab	0.64	0.09	0.7	0.01	0.3
NGC0289	SB(rs)bc	0.15	0.06	0.47	0.01	0.53
NGC4535	SAB(s)c	0.46	0.03	0.68	0.01	0.32
NGC6217	(R)SB(rs)bc	0.57	0.18	0.69	0.01	0.31
NGC6744	SAB(r)bc	0.24	0.01	0.61	0.01	0.39
ic1438	(R')SAB(rs)a:	0.29	0.02	0.54	0.01	0.46
NGC613	SB(rs)bc	0.52	0.06	0.68	0.01	0.32
NGC3198	SB(rs)c	0.19	0.02	0.5	0.01	0.5
NGC4421	SB(s)0/a	0.3	0.03	0.56	0.01	0.44
NGC5101	(R)SB(rs)0/a	0.44	0.01	0.59	0.01	0.41
NGC5371	SAB(rs)bc	0.31	0.03	0.58	0.01	0.42
NGC7329	SB(r)b	0.37	0.03	0.55	0.01	0.45

There is a sharp lower bound to the bar-axis ratio at $(b/a) \approx 0.28$. We believe this is an effect intrinsic to the bar geometry and not a selection bias due to the population of the sample. Menéndez-Delmestre et al. (2007) argue that stronger bars have a greater isophotal ellipticity than weaker bars. This trend however needs to be bounded, as extremely long and thin bars are not observed at any wavelength. Furthermore, gas and dust transport inside a bar places a physical limitation on the minimum value that the bar minor axis can be. This trend is evident even for bars that do not show very high values of Q_g, and suggests that this limitation to the bar-axis ratio is a fundamental property of the bar phenomenon itself.

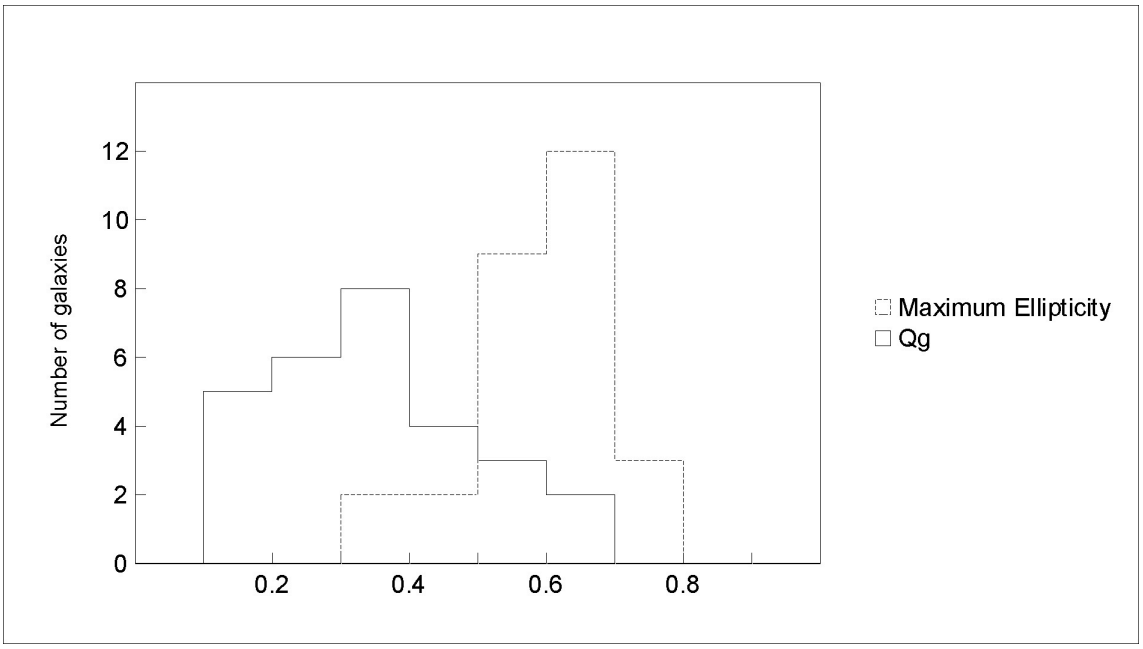

Figure 4.3: Number frequency of barred galaxies with bar strength defined in terms of maximum relative gravitational torque (solid line) and isophotal bar axis ratio, $b/a = 1 - \epsilon_{max}$ (dashed line). The results are consistent with our sample being biased towards nearby bright barred galaxies.

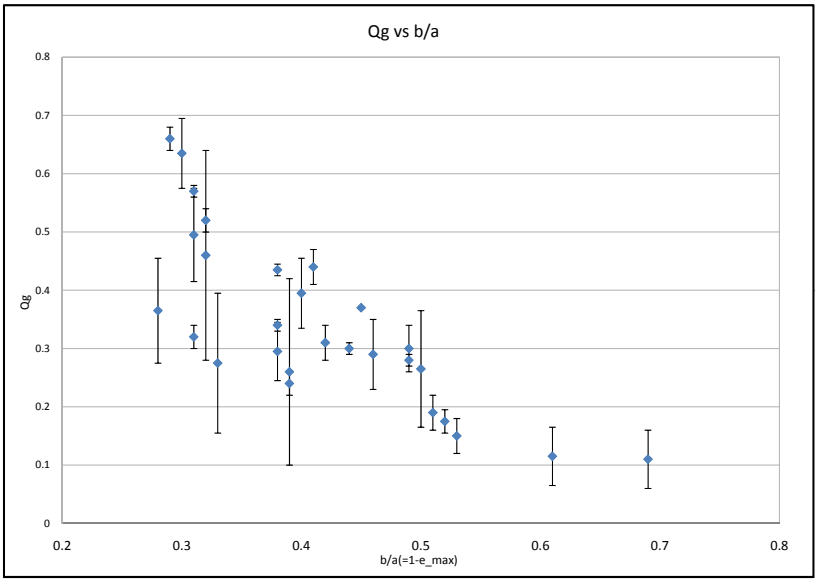

Figure 4.4: Comparison of maximum relative gravitational torques (Q_g) with maximum isophotal ellipticity values (ϵ_{max}). There is a good correlation between these bar strength measures for our sample where identical positions, deprojection and orientation parameters were used for each technique. The sharp minimum cutoff evident at $(b/a) \sim 0.3$ is attributed to the specific geometry of the bar phenomenon. Very long thin bars are not observed at any wavelength.

The non-axisymmetry of bars influences the large scale streaming motions of gas and dust. Athanassoula (1992) finds that the periodic orbits in barred galaxies are dependent on the central mass concentration of the barred galaxy model potential. In particular, a higher central mass concentration leads to more eccentric orbits, with larger curvature experienced at the orbits' apocenter. Furthermore, as bars become more narrow they become less massive.

Chapter 5

Conclusion

"The most beautiful thing we can experience is the mysterious. It is the source of all true art and science."
-Albert Einstein

"To raise new questions, new possibilities, to regard old problems from a new angle, requires creative imagination and marks real advance in science."
-Albert Einstein

5.1 Looking back

There was a time when galaxy morphology was a purely descriptive subject. Basic classes, such as ellipticals, spirals, irregulars and perhaps even S0's were the main players. The details of morphology and the detailed structures of galaxies were not considered important. Nor were the phenomena of bars and rings. Morphology without interpretation is essential early in the history of a discipline, but for it to truly mature into science, inferences from classification must be possible. Progress requires combining astrophysics with observed morphology and this requires a methodology, a system: a good classification scheme. The true purpose of a theory is twofold. Firstly, it should explain existing phenomena and observations. And secondly, it must be able to make specific predictions that can be verified with further observations. Reynolds had an elegant, yet deceptively simple, theory in mind when he suggested the notion of continuity between spiral disks. His scheme did not require a different classification for every galactic disk. He simply assumed an underlying structure for every galaxy and imagined how other galaxies would fit into that scheme. Interpretation is highly relevant in the longevity of a classification scheme. While Morgan invented a "simple"

scheme based on the central concentration of light in galaxies, the true survivor of early visual classification schemes is that of Reynolds and Hubble. Sandage argues that the prime reason Hubble's view has prevailed is because it does not account for every superficial detail, instead there is an overarching continuum along which the vast majority of nearby galaxies can be sorted. The graphical representation of this scheme, the famous "tuning fork diagram", suggested by Jeans and published by Hubble, has ensured its lasting success.

Having said this, there is only so much that can be accomplished by separating morphology and physics. Morphology and interpretation need to work together synergistically and objectively. Doing this successfully heralds the coming of age of a discipline. It is a two way street. Morphology relies on the guidance of theory to make sense of what is fundamental and what is not and theory needs to be grounded with objective maturity. Master of morphology, Gerard de Vaucouleurs was always supportive of a more objective approach by means of quantitative classification. By the early 1980's, theory had evolved enough to make some predictions about specific morphology which formed the groundwork for defining quantitative classification schemes. Descriptive (subjective) classification is intimately dependent on the human retina, and inherits the advantages and disadvantages that go along with that: an exquisite response to detail intricately tied up with the subjectivity of the human mind. However, quantitative morphology should *not* be a replacement for qualitative (classical) morphology - but merely a step to the next level.

This dissertation examined two quantitative approaches to galaxy classification at near infrared wavelengths. Relative gravitational torques were calculated for a sample of 40 nearby barred spiral galaxies with Spitzer IRAC $3.6\mu m$ and $4.5\mu m$ data, and were compared for image pairs of the same galaxy with identical position and orientation parameters. Secondly, isophotal ellipticities were calculated for a subsample of 28 warm mission S4G nearby barred spiral galaxies and provided a direct comparison of these two light flux quantitative classification schemes. This was followed by a discussion on the future of quantitative galaxy morphology and its place in contemporary extragalactic astrophysics.

5.2 Relative Maximum Gravitational Torques

An accurate distribution of maximum relative gravitational torques is derived for a sample of 40 3.6μm and 4.5μm Spitzer IRAC images. The sample is representative of nearby bright barred disks, but is biased against late-type, low-luminosity barred spirals. The distribution is instructive due to a wide range of inclination values and derived Q_g torques coinciding very well between the two passbands. The gravitational torque code is also a refinement of that used by Block et al. (2002). No bulge/disk decomposition has been used to carefully understand the effects of a change in wavelength from 3.6μm to 4.5μm on the morphology of the bulge region. The impact of bulge deprojection stretch however has been carefully considered and galaxies in the sample have not shown excessive deprojected bulge deformation. Orientation parameters are taken from the RC3 $logR_{25}$ axis-ratio parameter. With these refinements, an excellent agreement between 3.6μm and 4.5μm morphology is found. This provides an opportunity to classify intermediate redshift galaxies that have their 3.6μm rest frame emissions shifted red-ward to 4.5μm; i.e.: out to $z = 0.25$. A greater frequency of higher maximum relative torque galaxies compared to either Block et al. (2002) or Buta et al. (2004) is due to sample bias, as this dissertation is aimed at understanding quantitative methods in classifying *barred* galaxies. The implications for the observed bar fraction, and hence, the amount of accreted matter advocated by Block et al. (2002) remains to be evaluated. As the sample is biased towards high-luminosity systems, corrections for dark matter are expected to be small.

5.3 Isophotal Ellipses

The ellipse-fitting technique was successfully applied to a sample of 28 nearby barred galaxies imaged at 3.6μm from a subsample of S^4G. The histogram in Figure 4.3 shows the relative frequency of isophotal ellipses for a discrete set of axis-ratio $\epsilon = (1 - b/a)$ bins. The same sample of galaxies were subjected to the gravitational torque method as discussed extensively in Chapter 3. All orientation and deprojection parameters used were identical, which results in a bar strength correlation shown in Figure 4.4. The strength of bars as defined in terms of the gravitational torque parameter Q_g is confined within the limits $0 < Q_g < 1$. As such, bar axis ratios derived from the isophotal ellipse fitting method have been converted to $\epsilon = (1 - b/a)$. Block et al.

(2002) find a weak correlation between bar strength and the isophotal ellipse fitting method for a sample of 163 galaxies taken from the Ohio State University Bight Galaxy Survey (OSUBGS). Buta et al. (2004) find a better correlation of gravitational torque with isophotal ellipse fitting, a result these authors attribute to the use of a polar method for their gravitational torque analysis. The results in this dissertation support a strong correlation between gravitational torque method and isophotal ellipse fitting method, with the two analyses being subjected to the same galaxy sample with the same orientation parameters. This makes the correlation particularly instructive and suggests that an isophotal ellipse fitting approach to intermediate and high red-shift galaxies is in principle worth considering.

5.4 Future Focus

A powerful classification system does not have to be applicable to all galaxies, but it should be applicable to most. This includes galaxies at intermediate and high redshift. High redshift galaxies do not conform to the Hubble scheme. They are not Hubble types. The Hubble scheme, one of the most widely used classification schemes, is therefore not well suited to addressing the *formation* of galaxies. The kinds of galaxies that have existed in the past may have no counterparts today. And there may be galaxies today that have no counterparts in the past. This has resulted in a disconnect between nearby and high-z morphology. The key to bridging this gap is detecting observable evidence for galaxy *evolution*. i.e.: To observe morphological differences that are understood to be part of an evolutionary *sequence*. Furthermore, one of the most intriguing questions is how the bar fraction evolves *itself* over time? This question can be answered by studying bars out to $z \approx 0.25$. Rest-frame near infrared wavelengths would be shifted into the $4.5\mu m$ Spitzer passband at these redshifts, which is a quarter of the way back to the observable horizon.

5.5 Final words

Extragalactic morphology has emerged out of a series of advancements over the past few hundred years. The mysteries of structures and dynamics of the objects, initially known as “nebulae”, as well as their relation to one another, started to reveal themselves with the accumulation of data. As the mysteries of galaxy morphology started to unfold,

they led to an understanding of what galaxies are and how they evolved over time. Galaxies became fundamental units of matter in space. Galaxy morphology continues to be the backbone of extragalactic research even today. Astronomers, using space observations and advanced instruments, which can provide details of galactic structures over a wide range of distances and look back times, are still unmasking the secrets of galaxy structures. Despite the fact that the availability of advanced instruments and explosion of data has opened up new windows to be explored, classical morphology has not lost its relevance. Now more than ever, classical morphology is still a logical point for understanding galaxies.

Appendix A

Appendix

A.1 Image alignment & Cleaning

The initial steps in preparing the images for analysis are to align, and clean the images of any foreground stars. Aligning the images is achieved by obtaining the centres of galaxies using the IRAF routine IMEXAM and using these values as input parameters for IMLINTRAN. IMEXAM brings up a cursor that can manually be placed over the center of the galaxy in the image. Once this is done, pressing the "a" key and then the "q" key will display the center on the screen. Once all the centers for the sample galaxies have been obtained, the galaxies are then aligned. Finally they are resized to 600×600 with centre at $(300, 300)$.

Cleaning images of foreground stars is easy and quick with IRAF routines such as IMEDIT, PHOT, PSF, ALLSTAR, and SUBSTAR. However, the simplest approach in most cases is IMEDIT, unless large numbers of foreground stars need to be removed. To remove foreground stars we need to specify the radius of the circle, "+" increases the radius and "-" decreases it, and type "b". For exmaple:

```
imedit /ngc1300/ch1/ngc1300_1_maic.fits /ngc1300/ch1/ngc1300_1_c.fits
```

which will bring a cursor on the screen, place the cursor on a star and type "b", and increase/decrease radius as desired. Removing stars from the bright part of the galaxy may require the use of the IMEDIT routine more than once, as IMEDIT uses the parameters in the IRAF routine DISPLAY. It may be useful to set zrange and zscale to "no" and to fix values of z1 and z2 in order to see stars in the bright parts of a galaxy. However, this is not necessary for the stars around the galaxy image.

A.2 Image Scale and Size

The scale of the image can be found in the image header. The scale of the images used for analysis is typically 0.60 arcsec/pix.

```
imhead /ngc1300/ch1/ngc1300_1_maic.fits
```

In order to calculate the potential, QFG requires that all input images be square with an array dimension of 2^n, where n is an integer. Images used were all resized to 512×512 when deprojecting the images (see next section).

A.3 Deprojecting Images

Deprojecting images requires several parameters, such as position angle, logarithmic axis ratio and magnification factor. The values of position angle and logarithmic axis ratio can be obtained from the RC3. These values can then be used to deproject images using the IRAF routine IMLINTRAN as shown in the example below.

NGC1300 will be used to demonstrate the procedure of deprojection. The image is first star cleaned, centered, and then renamed to NGC1300_1_cc.fits. The value of xrotation and yrotation is determined by subtracting position angle from the CROTA2 value received from the image header. For NGC1300 the position angle is 106 and CROTA2 is -92.923200, giving the value of rotation to be -198.923200.

The magnification factor, also known as the apparent axis ratio, is calculated from the logarithmic axis ratio by $(10^{\log R_{25}})^{-1}$. From the RC3 we know that the logarithmic axis ratio for NGC1300 is given by $\log R_{25} = 0.18$, which corresponds to a magnification factor of 0.66. Using these parameters in IMLINTRAN the images can be deprojected. This routine will rotate the major axis to vertical and then stretch the pixels along the horizontal direction.

IMLINTRAN inputs for NGC1300:

```
input = ‘‘NGC1300_1_cc.fits’’ Input data
output = ‘‘NGC1300_1_deproj.fits" Output data
xrotation = -198.923200 X rotation angle in degrees
yrotation = -198.923200 Y rotation angle in degrees
xmag = 0.66 X output pixels per input pixel
```

```
ymag = 1 Y output pixels per input pixel
(xin = 300) X origin of input image in pixel
(yin = 300) Y origin of input image in pixel
(xout = 256) X origin of output image in pixels
(yout = 256) Y origin of output image in pixels
(ncols = 512) Number columns in the output image
(nlines = 512) Number lines in the output image
(interpolant = ‘‘linear")Interpolant(nearest,linear,poly3,poly5,spline3
(boundary = ‘‘constant")Boundary extension(nearest,constant,reflect,wr
(constant = 0.)  Constant for constant boundary extension
(fluxconserve = yes) Preserve image flux?
(nxblock = 512) X dimension of working block size in pixel
(nyblock = 512) Y dimension of working block size in pixel
(verbose = yes) Print messages about the progress of the task?
(mode = ‘‘ql")
```

To save the inputs and quit type “Ctrl + d ” then run IMLINTRAN.

Once the deprojection of all the images is accomplished, we need to rotate the images such that the bar of the galaxy image is horizontal. This can be done using the IRAF routine ROTATE.

Bibliography

Abraham, R. and Merrifield, M.: 2000, *AJ,* **120**, 2835

Abraham, R., Merrifield, M., Ellis, R., Tanvir, N., and Brinchmann, J.: 1999, *MNRAS,* **308**, 569

Abraham, R., Tanvir, N., Santiago, B., Ellis, R., Glazebrook, K., and van den Bregh, S.: 1996, *MNRAS* **279**, L47

Aguerri, J.: 1999, *A&A,* **351**, 43

Ann, H.: 2001, *JKAS,* **34**, S261

Ann, H. and Lee, H.: 2000, *JKAS,* **33**, 1

Athanassoula, E.: 1984, *Phys. Rep,* **114**, 319

Athanassoula, E.: 1992a, *MNRAS,* **259**, 328

Athanassoula, E.: 1992b, *MNRAS,* **259**, 345

Barazza, F., Jogee, S., and Marinova, I.: 2007, *IAUS,* **235**, 76

Berentzen, I., Athanassoula, E., Heller, C., and Fricke, K. J.: 2004, *MNRAS,* **347**, 220

Binney, J. and Tremaine, S.: 1987, *Galactic Dynamics*, Princeton: Princeton Univ. Press

Block, D., Bournaud, F., Combes, F., Puerari, I., and Buta, R.: 2002, *A&A,* **394**, L35

Block, D., Buta, R., Knapen, J. H., Elmegreen, B. G., Elmegreen, D. M., and Puerari, I.: 2004a, *AJ,* **128**, 183

Block, D. and Freeman, K.: 2008, *Shrouds of the night: masks of the Milky Way and our awesome new view of galaxies*, Springer

Block, D. and Puerari, I.: 1999, *A&A,* **342**, 627

Block, D. L., Bertin, G., Stockton, A., Grosbol, P., Moorwood, A. F. M., and Peletier, R. F.: 1994, *A&A,* **288**, 365

Block, D. L., Freeman, K. C., Jarret, T. H., Puerari, I., Worthey, G., Combes, F., and Groess, R.: 2004b, *A&A,* **425**, 37

Block, D. L., Puerari, I., Knapen, J. H., Elmegreen, B. G., Buta, R., Stedman, S., and Elmegreen, D. M.: 2001, *A&A,* **375**, 761

Block, D. L., Stockton, A., Elmegreen, B. G., and Willis, J.: 1999, *ApJ,* **522**, L25

Bournaud, F. and Combes, F.: 2002, *A&A,* **392**, 83

Bournaud, F. and Combes, F.: 2003, *A&A,* **401**, 817

Bournaud, F. and Combes, F.: 2004, Bar dissolution and reformation mechanisms, in D. L. Block, I. Puerari, K. C. Freeman, R. Groess, & E. K. Block (ed.), *Penetrating*

Bars Through Masks of Cosmic Dust, Vol. 319 of *Astrophysics and Space Science Library*, p. 165

Buta, R.: 1986, *ApJS,* **61**, 631

Buta, R.: 1995, *ApJS,* **96**, 39

Buta, R.: 2002, *ASP COnf. Ser.,* **275**, 185

Buta, R. and Block, D. L.: 2001, *ApJ,* **550**, 243

Buta, R., Block, D. L., and Knapen, J. H.: 2003a, *AJ,* **126**, 1148

Buta, R., Byrd, G., and Freeman, T.: 2003b, *AJ,* **125**, 634

Buta, R. and Combes, F.: 1996, *Fundamentals of Cosmic Physics,* **17**, 95

Buta, R., Laurikainen, E., and Salo, H.: 2004, *AJ,* **127**, 279

Buta, R., Vasylyev, S., Salo, H., and Laurikainen, E.: 2005, *AJ,* **130**, 506

Buta, R. J.: 2011, *Galaxy Morphology*, 6, ed. T. Oswalt, in press, arXiv 1102.0550

Chapelon, S., Contini, T., and Davoust, E.: 1999, *A&A,* **345**, 81

Combes, F. and Elmegreen, B. G.: 1993, *A&A,* **271**, 391

Combes, F. and M.Gerin: 1985, *A&A,* **150**, 327

Combes, F. and Sanders, R. H.: 1981, *A&A,* **96**, 164

Comerön, S., Martinez-Valpuesta, I., Knapen, J. H., and Beckman, J. E.: 2009, *ApJ,* **706**, L256

Cooley, J. and Tukey, J.: 1965, *Math. Computat.* **19**, 297

Curtis, H. D.: 1918a, *Publ.Lick Obs.,* **13**, 12

Curtis, H. D.: 1918b, *Descriptions of 762 nebulae and clusters photographed with the Crossley reflector. Publications of the Lick Observatory,* **XIII**, 11

Curtis, H. D.: 1918c, *A Study of Occulting Matter in the Spiral Nebulae. Publications of the Lick Observatory,* **XIII**, 45

Das, M., Teuben, P., Vogel, S. N., Regan, M. W., Sheth, K., Harris, A. I., and Jefferys, W. H.: 2003, *ApJ,* **582**, 190

de Grijs: 1998, *MNRAS,* **299**, 59

de Vaucouleurs, G.: 1956, *Mem. Commonw. Obs. (Mount Stromlo),* **3**, No. 13

de Vaucouleurs, G.: 1959, *ApJ,* **130**, 728

de Vaucouleurs, G.: 1963, *ApJS,* **8**, 31

de Vaucouleurs, G. and de Vaucouleurs, A.: 1959, *PASP,* **71**, 83

de Vaucouleurs, G. and de Vaucouleurs, A.: 1963, *AJ,* **68**, 278

de Vaucouleurs, G., de Vaucouleurs, A., Corwin, H. G., Buta, R. J., Paturel, G., and Fougue, P.: 1991, *'Third Reference Catalogue of Bright Galaxies'*, Volume 1-3, XII (Springer-Verlag Berlin Heidelberg New York)

Dickinson, M., Giavalisco, M., and GOODS Team: 2003, The Great Observatories Origins Deep Survey, in R. Bender & A. Renzini (ed.), *The Mass of Galaxies at Low and High Redshift*, p. 324

Disney, M. J., Davies, J., and Phillips, S.: 1989, *MNRAS,* **239**, 939

Draine, B. T. and Li, A.: 1984, *ApJ* **285**, 89

Draine, B. T. and Li, A.: 2007, *ApJ,* **657**, 810

Dreyer, J. L. E.: 1888, *memras,* **49**, 1, A New General Catalogue of Nebulae and Clusters of Stars,being the Catalogue of the late Sir John F.W. Herschel, Bart., revised, corrected, and enlarged.

Elmegreen, B. G. and Elmegreen, D. M.: 1985, *ApJ,* **288**, 438

Elmegreen, B. G., Elmegreen, D. M., and Hirst, A. C.: 2004, *ApJ,* **612**, 191

Elmegreen, B. G., Galliano, E., and Alloin, D.: 2009, *AJ* **703**, 1297

Elmegreen, D. M., Chromey, F. R., Bissell, B. A., and Corrado, K.: 1999, *AJ,* **118**, 2618

Elmegreen, D. M. and Elmegreen, B. G.: 1982, *MNRAS,* **201**, 1021

Elmegreen, D. M. and Elmegreen, B. G.: 1987, *ApJ,* **314**, 3

Elmegreen, D. M., Elmegreen, B. G., Chromey, F. R., Hasselbacher, D. A., and Bissell, B. A.: 1996, *AJ,* **111**, 1880

Emsellem, E., Goudfrooil, P., and Ferruit, P.: 2003, *MNRAS,* **345**, 1297

Erwin, P.: 2005, *MNRAS,* **364**, 283

Eskridge, P. B. and Frogel, J. A.: 1999, *Astrophysics & Space Science,* **269**, 427

Eskridge, P. B., Frogel, J. A., Pogge, R. W., Quillen, A., Davies, R., DePoy, D., Houdashelt, M., Kuchinski, L., Ramírez, S., Sellgren, K., Terndrup, D., and Tiede, G.: 2000, *AJ,* **119**, 536

Eskridge, P. B., Frogel, J. A., Pogge, R. W., Quillen, A. C., Berlind, A. A., Davies, R. L., DePoy, D. L., Gilbert, K. M., Houdashelt, M. L., Kuchinski, L. E., Ramírez, S. V., Sellgren, K., Stutz, A., Terndrup, D. M., and Tiede, G. P.: 2002, *ApJS* **143**, 73

Fazio, G. G., Hora, J. L., Allen, L. E., Ashby, M. L. N., Barmby, P., Deutsch, L. K., Huang, J.-S., Kleiner, S., Marengo, M., Megeath, S. T., Melnick, G. J., Pahre, M. A., Pattern, B. M., Polizotti, J., Smith, H. A., Taylor, R. S., Wang, Z., Willner, S. P., Hoffmann, W. F., Pipher, J. L., Forrest, W. J., McMurty, C. W., McCreight, C. R., McKelvey, M. E., McMurray, R., Koch, D., Moseley, S., Arendt, R., Mentzell, J., Marx, C., Losch, P., Mayman, P., Eichhorn, W., Krebs, D., Jhabvala, M., Gezari, D., Fixsen, D., Flores, J., Shakoorzadeh, K., Jungo, R., Hakun, C., Workman, L.,

Karpati, G., Kichak, R., Whitley, R., S.Mann, Tollestrup, E. V., Eisenhardt, P., Stern, D., Gorjian, V., Bhattacharya, B., Carey, S., Nelson, B., Glaccum, W., Lacy, M., Lowrance, P. J., Laine, S., Reach, W., Stauffer, J., Surace, J., Wilson, G., Wright, E., Hoffman, A., Domingo, G., and M.Cohen: 2004, *ApJS,* **154**, 10

Förster Schreiber, N. M., Genzel, R., Bouché, N., Cresci, G., Davies, R., Buschkamp, P., Shapiro, K., Tacconi, L. J., Hicks, E. K. S., Genel, S., Shapley, A. E., Erb, D. K., Steidel, C. C., Lutz, D., Eisenhauer, F., Gillessen, S., Sternberg, A., Renzini, A., Cimatti, A., Daddi, E., Kurk, J., Lilly, S., Kong, X., Lehnert, M. D., Nesvadba, N., Verma, A., McCracken, H., Arimoto, N., Mignoli, M., and Onodera, M.: 2009, *ApJ* **706**, 1364

Freeman, K. C.: 1989, *in Gerard and Antoinette de Vaucouleurs: A Life for Astronomy. Advanced Series in Astrophysics and Cosmology* **4**, 85

Frogel, J. A., Quillen, A. C., and Pogge, R. W.: 1996, *in New Extragalactic Perspective in the New South Africa,* p. 65

Greenberg, J. M. and Li, A.: 1996, *in New Extragalactic Perspective in the New South Africa,* p. 118

Groess, R.: 2007, *Gravitational Torques Of The Dust Penetrated Stellar Backbone of Extragalactic Spiral Disk*, *Ph.D. thesis*, University Of Witwatersrand

Hackwell, J. A. and Schweizer, F.: 1983, *ApJ,* **265**, 643

Hasan, H. and Norman, C. A.: 1990, *ApJ,* **361**, 69

Hasan, H., Pfenniger, D., and Norman, C.: 1993, *ApJ,* **409**, 91

Herschel, J. F. W.: 1864, *Philosophical Transactions of the Royal Society of London,* **154**, 1

Herschel, W.: 1912, In Scientific Papers of Sir William Herschel, 2 Vols. London: R. Astron. Soc.

Ho, L. C., Filippenko, A. V., and Sargent, W. L. W.: 1997a, *ApJS,* **112**, 315

Ho, L. C., Filippenko, A. V., and Sargent, W. L. W.: 1997b, *ApJ,* **487**, 591

Hohl, F. and Hockney, R.: 1969, *Journal of Computational Physics,* **4**, 306

Hozumi, S. and Hernquist, L.: 1999, *in "Galaxy Dynamics", ASP Conf Series,* **185**, 259

Hubble, E.: 1922, *AJ,* **56**, 162

Hubble, E.: 1926, *AJ,* **64**, 321

Hubble, E.: 1927, *Observatory,* **50**, 276

Hubble, E.: 1936, *Realm of the Nebulae*, New Heaven : Yale Univ. Press

Huntley, J. M.: 1978, *ApJ,* **225**, 101

Jarrett, T. J., Chester, T., Cutri, R., Schneider, S. E., and Huchra, J. P.: 2003, *AJ,* **125**, 525

Jeans, J.: 1919, *Problems of Cosmogony and Stellar Dnamics*, Cambridge: Cambridge Univ. Press

Jeans, J.: 1929, *Astronomy and Cosmogony*, Cambridge: Cambridge Univ. Press

Jedrzejewski, R.: 1987, *MNRAS,* **226**, 747

Jogee, S., Barazza, F., Rix, H.-W., Shlosman, I., Barden, M., Wolf, C. W., Davies, J., Heyer, I., Beckwith, S. V. W., Bell, E. F., and et. al.: 2004, *ApJ,* **615**, L105

Jogee, S., Conselice, C., Ravindranath, S., Shlosman, I., Knapen, J. H., Mobasher, B., Koekemoer, A. M., Lucas, R. A., Laine, S., Hornschemeier, A., and GOODS Team: 2002, Structure and Evolution of Disk Galaxies in the GOODS Fields, in *American Astronomical Society Meeting Abstracts*, Vol. 201 of *Bulletin of the American Astronomical Society,*, p. 615

Jogee, S., Kenney, J. D. P., and Smith, B. J.: 1999, *ApJ,* **526**, 665

Jogee, S., Knapen, J., Shlosman, I., Englmaier, P., Laine, S., Scoville, N., and Wilson, C.: 2002, The Extended Bar and Grand-Design Spirals in NGC 5248, in E. Athanassoula, A. Bosma, & R. Mujica (ed.), *Disks of Galaxies: Kinematics, Dynamics and Peturbations*, Vol. 275 of *Astronomical Society of the Pacific Conference Series,*, p. 275

Junqueira, S. and Combes, F.: 1996, *A&A,* **312**, 703

Kennicutt, R. C., Bendo, G., Engelbracht, C., Gordon, K., Li, A., Rieke, G. H., Rieke, M. J., Smith, J. D., Armus, L., Helou, G., Jarrett, T. H., Roussel, H., Calzetti, D., Leitherer, C., Malhotra, S., Meyer, M., Regan, M. W., Dale, D. A., Draine, B., Grauer, A. D., Hollenbach, D. J., Kewley, L. J., Murphy, E., Thornley, M. D., and Walter, F.: 2003, SINGS: The SIRTF Nearby Galaxies Survey, in *American Astronomical Society Meeting Abstracts*, Vol. 35 of *Bulletin of the American Astronomical Society,*, p. 1351

Kent, S.: 1983, *ApJ,* **266**, 562

Knapen, J. H., Shlosman, I., and Peletier, R. F.: 2000, *ApJ,* **529**, 93

Knox-Shaw, H.: 1915, *Helwan Obs. Bull.*, **15**, 129

Kormendy, J.: 1979, *ApJ,* **227**, 714

Kormendy, J. and Kennicutt, R. C.: 2004, *Annual Review of Astronomy & Astrophysics,* **42**, 603

Kormendy, J. and Norman, C.: 1979, *ApJ,* **223**, 539

Laine, S., Shlosman, I., Knapen, J. H., and Peletier, R. F.: 2002, *ApJ,* **567**, 97

Laurikainen, E. and Salo, H.: 2002, *MNRAS,* **337**, 1118

Laurikainen, E., Salo, H., and Buta, R.: 2004, *ApJ,* **607**, 103

Laurikainen, E., Salo, H., and Rautiainen, P.: 2002, *MNRAS,* **331**, 880

Lin, C. C.: 1971, *Highlights of Astronomy* **2**, 88

Lundmark, K.: 1926, *Ark. Math. Astron. Phys. Ser. B,* 19, No.8

Lundmark, K.: 1927, *Medd. Astron. Obs. Uppsala,*, No.30

Marinova, I. and Jogee, S.: 2007, *ApJ,* **659**, 1176

Martin, P.: 1995, *AJ,* **109**, 2428

Martin, P. and Friedli, D. F.: 1997, *A&A,* **326**, 449

Martin, P. and Roy, J. R.: 1994, *ApJ,* **424**, 599

McCall, M. L.: 1986, *PASP,* **98**, 992

Menéndez-Delmestre, K., Sheth, K., Schinnerer, E., Jarrett, T. H., and Scoville, N. Z.: 2007, *ApJ,* **657**, 790

Miller, R. H.: 1996, *in ASP Conf. Ser. 91, Barred Galaxies,* p. 569

Miller, R. H., Prendergast, K. H., and Quirk, W. J.: 1970, *ApJ,* **161**, 903

Miwa, T. and Noguchi, M.: 1998, *ApJ,* **499**, 149

Morgan, W. W.: 1958, *PASP,* **70**, 364

Mulchaey, J. S. and Regan, M. W.: 1997, *ApJ,* **482**, L135

Noguchi, M.: 1996, *ApJ,* **469**, 605

Norman, C. A., Sellwood, J. A., and Hasan, H.: 1996, *ApJ,* **462**, 114

Ohta, K., Hamabe, M., and Wakamatsu, K.-I.: 1990, *ApJ,* **357**, 71

Pahre, A., Asby, M., Fazio, G., and Willner, S.: 2004, *ApJS,* **154**, 229

Peng, C., Ho, L., Impey, C., and Rix, H.-W.: 2002, *AJ,* **124**, 266

Persic, M., Salucci, P., and Stel, F.: 1996, *MNRAS,* **281**, 27

Pfenniger, D., Combes, F., and Martinet, L.: 1996, *in 'New Extragalactic Perspectives in the New South Africa',* p. 291

Pfenniger, D. and Norman, C.: 1990, *ApJ,* **363**, 391

Piner, B., Stone, J. M., and Teuben, P. J.: 1995, *ApJ,* **449**, 508

Prendergast, K. H.: 1962, *IAUS,* **15**, 126

Prendergast, K. H.: 1983, *IAUS,* **100**, 215

Quillen, A. C., Frogel, J. A., and González, R. A.: 1994, *ApJ,* **437**, 162

Regan, M. W. and Elmegreen, D. M.: 1997, *AJ,* **114**, 965

Regan, M. W., Sheth, K., and Vogel, S. N.: 1999, *ApJ,* **526**, 97

Regan, M. W. and Teuben, P. J.: 2004, *ApJ,* **600**, 595

Regan, M. W., Vogel, S. N., and Teuben, P. J.: 1997, *ApJ,* **482**, L143

Reynolds, J. H.: 1920, *MNRAS,* **80**, 746

Reynolds, J. H.: 1927, *Observatory,* **50**, 185,308

Rieke, G. and Lebofsky, M. J.: 1985, *ApJ,* **288**, 618

Rix, H.-W., Beckwith, M. B. S., Bell, E., Borch, A., Caldwell, J., Haussler, B., Jahke, K., Jogee, S., McIntosh, D. H., Meisenheimer, K., Peng, C., Sebastian, S., R.S.Somerville, Wisotzki, L., and Wolf, C.: 2004, *ApJs,* **152**, 163

Rix, H.-W. and Rieke, M. J.: 1993, *ApJ,* **418**, 123

Roberts, W. W., Roberts, M. S., and Shu, F. H.: 1975, *ApJ,* **196**, 381

Rozas, M., Kanpen, J. H., and Beckman, J. E.: 1998, *MNRAS,* **301**, 631

Sakamoto, K., Okumura, S. K., Ishizuki, S., and Scoville, N. Z.: 1999, *ApJ,* **525**, 691

Sandage, A.: 1961, *Hubble Atlas of Galaxies*, p. 618

Sandage, A.: 1975, *Stars and Stellar Systems*, **9**, 1

Sandage, A.: 2005, *Annu. Rev. Astron. Astrophys.,* **43**, 581

Sandage, A. and Bedke, J.: 1994, *The Carnegie Atlas of Galaxies, Carnegie Institute of Washington Publication,*, No. 638

Sanders, R. H. and Tubbs, A. D.: 1980, *ApJ,* **235**, 803

Schwarz, M. P.: 1981, *ApJ,* **247**, 77

Scoville, N. Z., Matthews, K., Carico, D. P., and Sanders, D. B.: 1988, *ApJ,* **327**, L61

Scoville, N. Z. and Team, C.: 2007, *ApJS,* **172**, 150

Seigar, M. S. and James, P. A.: 1998, *MNRAS,* **299**, 672

Sellwood, J. and Wilkinson, A.: 1993, *Rep. Prog. Phys.,* **56**, 173

Sellwood, J. A.: 1996, *in ASP Conf. Ser. 91, Barred Galaxies* p. 259

Sellwood, J. A.: 2000, *ASP Conf. Ser.* **197**, 3

Sellwood, J. A. and Moore, E. M.: 1999, *ApJ,* **510**, 125

Semelin, B. and Combes, F.: 2002, *A&A,* **388**, 826

Shapley, H. and Curtis, H. D.: 1921, *Bull. Nat. Res. Council,* **2**, 217

Shen, J. and Sellwood, J. A.: 2004, *ApJ,* **604**, 614

Sheth, K., Manéndez-Delmestre, K., Scoville, N., Jarrett, T., Strubbe, L., Regan, M. W., Schinnerer, E., and Block, D. L.: 2004, *in Penetrating Bars Through Masks of Cosmic Dust,* **319**, 405

Sheth, K., Regan, M. W., Scoville, N. Z., and Strubbe, L. E.: 2003, *ApJ,* **592**, L13

Sheth, K., Regan, M. W., Vogel, S. N., and Teuben, P. J.: 2000, *ApJ,* **532**, 221

Sheth, K., Vogal, S. N., Regan, M. W., Thornley, M. D., and Teuben, P. J.: 2005, *ApJ,* **632**, 217

Sheth, K., Vogel, S. N., Regan, M. W., Teuben, P. J., Harris, A. I., and Thornley,

M. D.: 2002, *AJ,* **124**, 2581

Shlosman, I., Frank, J., and Begelman, M. C.: 1989, *Nature,* **338**, 45

Shlosman, I., Peletier, R. F., and Knapen, J. H.: 2000, *ApJL* **535**, L83

Slipher, V. M.: 1917, *Proceedings of the American Philosophical Society,* **56**, 403

Stebbins, J., Huffer, C. M., and Whitford, A. E.: 1939, *ApJ,* **90**, 209

Teuben, P.: 1995, *in ASP Conf. Ser. 77, Astronomical Data Analysis Software and Systems iV* p. 398

Thronson, H. A., Harley, A., Hereld, M., Majewski, S., Greenhouse, M., Johnson, P., Spillar, E., Woodward, C. E., Harper, D. A., and Rauscher, B. J.: 1989, *ApJ,* **343**, 158

Tokunaga, A. T., Sellgren, K., Smith, R. G., Nagata, T., Sakata, A., and Nakada, Y.: 1991, *ApJ,* **380**, 452

Trumpler, R. J.: 1930, *Preliminary results on the distances, dimensions and space distribution of open star clusters, Lick OBs. Bull. XIV,* p. 154

Tully, R. B.: 1988, *Nearby galaxies catalog*

Tully, R. B. and Fisher, J. R.: 1987, *Atlas of Nearby Galaxies*

Valentijn: 1990, *Nature,* **346**, 153

van Albada, G. D. and Roberts, W.: 1981, *ApJ,* **246**, 740

van de Hulst, H. C.: 1949, *Nature,* **163**, 24

van den Bergh, S.: 1960, *ApJ,* **131**, 215

Vorontsov-Velyaminov, B. A., Krasnogorskaja, A., and Arkipova, V. P.: 1962-1974, *Morphological Catalogue of Galaxies*, 1-5, Moscow

Whitford, A. E.: 1948, *ApJ,* **107**, 102

Whyte, L. F., Abraham, R. G., Merrifield, M. R., Eskridge, P. B., Frogel, J. A., and Pogge, R. W.: 2002, *MNRAS,* **336**, 1281

Wijesinghe, D., Hopkins, A. M., Kelly, B. C., N.Welikala, and Connolly, A. J.: 2009, *MNRAS,* pp 1–11

Witt, A. N., Thronson, Jr., H. A., and Capuano, Jr., J. M.: 1992, *ApJ,* **393**, 611

Wolf, M.: 1908, *Publ. Astrophys. Inst. König. Heidelberg,* 3(3)

Wozniak, H., Combes, F., Emsellem, E., and Friedli, D.: 2003, *A&A,* **409**, 463

Wozniak, H. and Pierce, M. J.: 1991, *A&AS,* **88**, 325

Young, P. J., Kristian, J., Westphal, J. A., and Sargent, W. L. W.: 1979, *ApJ,* **234**, 76

Zheng, X. Z., Hammer, F., Flores, H., Assémat, F., and Rawat, A.: 2005, *A&A,* **435**, 507